Quaternary Science Reviews 375 (2026) 109755

Contents lists available at ScienceDirect

Quaternary Science Reviews

journal homepage: www.elsevier.com/locate/quascirev

Bipolar volcanic ice-core synchronization of the entire last glacial period

Anders Svensson [a,*], Guido Vettoretti [a], Jia-mei Lin [a], Giulia Sinnl [a], Dorthe Dahl-Jensen [a], Jørgen Peder Steffensen [a], Sune Olander Rasmussen [a], Bo Vinther [a], Christine Hvidberg [a], Helle Astrid Kjær [a], Vasileios Gkinis [a], Eliza Cook [a], Johannes Lohmann [a], Jonathan Ortved Melcher [a], Sune Halkjær [a], Sepp Kipfstuhl [b], Frank Wilhelms [b,c], Florian Adolphi [b,d], Hubertus Fischer [e], Matthias Bigler [e], Michael Sigl [e], Amaelle Landais [f], Marie Bouchet [f], Anna Klüssendorf [a,f], Frédéric Parrenin [g], Robert Mulvaney [h], Eric Wolff [i], Andrea Burke [j], Helen Innes [j], Mirko Severi [k], Christo Buizert [l], Joseph R. McConnell [m], Nathan Chellman [m], Sophia Wensman [m], Jürg Beer [n], Ikumi Oyabu [o], Raimund Muscheler [p]

[a] Physics of Ice, Climate and Earth, Niels Bohr Institute, University of Copenhagen, Copenhagen, Denmark
[b] Stiftung Alfred-Wegener-Institut für Polar- und Meeresforschung, Bremerhaven, Germany
[c] Geowissenschaftliches Zentrum Universität Göttingen, Göttingen, Germany
[d] Faculty of Geosciences, Bremen University, Bremen, Germany
[e] Climate and Environmental Physics, Physics Institute & Oeschger Centre for Climate Change Research, University of Bern, Bern, Switzerland
[f] Laboratoire des Sciences du Climat et de l'Environnement, IPSL, UMR 8212, CEA-CNRS-UVSQ-UPS, Gif sur Yvette, France
[g] Université Grenoble Alpes, CNRS, INRAE, IRD, Grenoble INP, IGE, Grenoble, France
[h] British Antarctic Survey, Cambridge, UK
[i] Department of Earth Sciences, University of Cambridge, UK
[j] School of Earth and Environmental Sciences, University of St Andrews, St Andrews, UK
[k] Department of Chemistry "Ugo Schiff", University of Florence, Florence, Italy
[l] College of Earth, Ocean and Atmospheric Sciences, Oregon State University, Corvallis, OR, USA
[m] Division of Hydrologic Sciences, Desert Research Institute, Reno, NV, USA
[n] Eawag, Dübendorf, Switzerland
[o] National Institute of Polar Research, Tokyo, Japan
[p] Department of Geology, Lund University, Lund, Sweden

ARTICLE INFO

Handling editor: Qiuzhen Yin

ABSTRACT

Precise synchronization of paleoclimate records is essential for inferring the dynamics and past evolution of the climate system. For the last glacial period, the time scales of ice cores from the Greenland and Antarctic ice sheets have been synchronized by the use of cosmogenic radionuclides, atmospheric gas concentrations, and traces of large volcanic eruptions. Here we identify the sulfate deposition signatures of the same 300 volcanic eruptions in different Greenland and Antarctic ice cores to obtain an inter-hemispheric volcanic ice-core synchronization of the entire last glacial period and the early Holocene (10–110 ka). Compared to earlier bipolar volcanic synchronizations, we close a gap in the period 16.5–24.5 ka and extend the synchronization to cover the 10–12 ka and 60–110 ka intervals. Furthermore, we increase the density of bipolar match points and make updates and corrections of the existing bipolar and unipolar synchronizations. The volcanic synchronization is in agreement with existing bipolar synchronizations from independent ^{10}Be and methane matching. The bipolar volcanic synchronization allows us to determine the precise phasing of interhemispheric abrupt climate events throughout the last glacial period, particularly those associated with Dansgaard-Oeschger (D-O) events. Our improved synchronization and extended time period allow us to show that at the time of the D-O warming transitions, the average Antarctic temperature reaches a maximum within decades after the Greenland temperature maximum. This rapid Antarctic warming is superimposed on the well-known millennial-scale thermal bipolar-seesaw warming in Antarctica commonly attributed to oceanic heat transport and confirms earlier work that the abrupt change observed in Greenland is associated with a direct atmospheric circulation change at a global scale.

* Corresponding author.
E-mail address: as@nbi.ku.dk (A. Svensson).

https://doi.org/10.1016/j.quascirev.2025.109755
Received 13 May 2025; Received in revised form 2 December 2025; Accepted 15 December 2025

The exception to this pattern occurs for the EDML ice-coring site located in the Atlantic sector of Antarctica, potentially related to sea-ice conditions in the Weddell Sea. Comparison to state-of-the-art climate model simulations shows excellent agreement in the overall bipolar climate phasing at the warming transitions and allows for analysis of the climate-system behavior at those transitions. The model simulations suggest that the abrupt Antarctic warming response observed is connected with an interhemispheric atmospheric response involving a global scale reorganization of the zonal mean atmospheric circulation. The abrupt D-O surface warming signal in the Northern Hemisphere is teleconnected into an abrupt Antarctic surface warming through changes in the Southern Hemisphere eddy-driven jet and anomalous circulation changes in the associated Ferrel and Polar cells.

1. Introduction

The quest for synchronization of paleoclimate records covering the last glacial period is an ongoing effort that involves a number of different natural archives, such as marine and lake sediments, corals, speleothems, tree rings, and ice cores. With their high temporal resolution, complete coverage of the last glacial cycle, and precise linking to climate records from many other paleoclimate archives, ice cores from Greenland (Kalaallit Nunaat) and Antarctica provide a unique opportunity to determine the coupling of the last glacial climate evolution in the two hemispheres at decadal precision. In particular, the climatic evolution of the last glacial period, for which bipolar ice-core records exist, is of greatest importance to study abrupt climate events, known as Dansgaard-Oeschger (D-O) events that have different expressions in the two hemispheres (Buizert, 2023; EPICA community members, 2006). Abrupt climate-change events in the past are relevant for the study of future global-warming scenarios where some of the major elements of the climate system may experience 'tipping' or abrupt changes of similar magnitude and speed as those observed in the last glacial period (McKay et al., 2022; Wang et al., 2023).

Existing synchronizations of the Greenland and Antarctic climate signals in the last glacial period include those based on methane concentrations (Blunier et al., 1998; EPICA community members, 2006; Lemieux-Dudon et al., 2010; Martin et al., 2023; Rhodes et al., 2015; WAIS Divide Project Members, 2015), isotopic composition of O_2 in air bubbles (Bender et al., 1994; Capron et al., 2010b), cosmogenic radionuclides (Raisbeck et al., 2007, 2017; Sinnl et al., 2023), and global volcanism (Svensson et al., 2013, 2020). All synchronization methods have their strengths and weaknesses. The methane approach enables synchronization at the abrupt warming transitions where the global atmospheric concentration changes abruptly, but it suffers from uncertainties related to the age difference between gasses and the ice at the same depth, known as the gas-age–ice-age difference, or Δage (Schwander and Stauffer, 1984). Bipolar cosmogenic synchronization is precise, but limited by weather/climate noise affecting the radionuclide data and the quasi-cyclic nature of solar activity changes, leaving a repeated pattern in the cosmogenic isotope fluxes that may allow for multiple non-unique matches. Further, most cosmogenic isotope records do not possess sufficient resolution to resolve annual or even decadal events during the glacial. The matching is therefore most reliable during periods of significant and rare events such as the Laschamps event or strong solar energetic particle events (e.g., Sigl et al. (2015)) or in combination with stratigraphic information. The volcanic bipolar synchronization approach can be applied when a series of large volcanic eruptions can be identified as peaks in acidity or sulfate concentration at both poles from their relative temporal separation. To obtain precise bipolar synchronizations, all of the methods require the availability of high-resolution records from both Greenland and Antarctica.

The coupling of inter-hemispheric climate evolution related to the last-glacial abrupt climate events is a topic of particular interest, as it is a prerequisite for deciphering the global dynamics of those climate events. Greenland and Antarctic ice cores provide a unique opportunity for studying this coupling of global climate at a decadal scale over the entire last glacial cycle (Landais et al., 2015). Existing bipolar ice-core synchronizations have supported the existence of an ocean-driven thermal bipolar seesaw mechanism (Stocker and Johnsen, 2003) in which the state of North Atlantic deep-water formation and the associated Atlantic Ocean circulation alters the delivery of heat to higher latitudes of the two hemispheres on a centennial-to-millennial time scale. The thermal bipolar seesaw leads to a characteristic interpolar climate pattern, in which Antarctic records are gradually warming when Greenland is in a cold climatic period (Greenland stadial, GS) and Antarctica is cooling when Greenland is in a mild period (Greenland interstadial, GI). Mathematically, on millennial timescales, Greenland temperature is strongly anti-correlated with the time derivative of Antarctic temperature. The idea of a thermal bipolar seesaw involving mean ocean temperature (MOT) has been recently proposed as a conceptual model of the ocean teleconnection between the poles (Buizert, 2023; Pedro et al., 2018).

Going beyond the millennial-scale expression of D-O cycles at both poles, increased precision in the bipolar synchronization fostered studies on the immediate Antarctic temperature signal associated with the rapid Greenland D-O warmings, which is superimposed on the multi-centennial to millennial bipolar seesaw warming. WAIS Divide Project Members (2015) used bipolar methane concentration matching of the Antarctic WD and the Greenland NGRIP ice cores to determine an average 210 ± 100 yr time-lag for West Antarctica to reach the transition from a warming to a cooling trend, relative to the midpoint of Greenland warming. Based on the same synchronization but looking at the Deuterium excess (Dx) record rather than $\delta^{18}O$, Markle et al. (2016) found a faster Antarctic response time compared to that of $\delta^{18}O$. The onset of the WD Dx change is essentially synchronous to the onset of the D-O warming in the North but takes longer to reach its maximum than the corresponding D-O warming in Greenland. Using the same bipolar methane synchronization, and a new volcanic synchronization between Antarctic ice cores, Buizert et al. (2018) showed that the synchronous Dx response is seen across Antarctica, and that several East Antarctic cores exhibit an abrupt $\delta^{18}O$ response that is synchronous with Northern Hemisphere D-O activity and superimposed on the millennial-scale thermal bipolar seesaw signal. These general ideas tend to explain much of the variability and correlation between ice-core data from Greenland and Antarctica on millennial timescales. With the introduction of more precise bipolar volcanic synchronization in the 12–60 ka period, Svensson et al. (2020) refined the Antarctic time lag for the onset of Antarctic average $\delta^{18}O$ cooling relative to the midpoint of Greenland warming via the thermal bipolar seesaw to be 120 ± 24 yr. When making a composite (or stack) of Dx from multiple D-O events, the reconstructed Antarctic response is much more abrupt in the bipolar volcanic synchronization than in the methane synchronization, suggesting that in the latter method, individual events are not as well aligned due to the lower precision of the method. In both bipolar synchronization methods, the Atlantic–facing EDML ice-coring site represents an exception to Antarctic-wide $\delta^{18}O$ trends, showing a cooling trend at the time of the Greenland warming.

A gradual Antarctic warming and century-long time-lag in the Antarctic-wide bipolar seesaw $\delta^{18}O$ response to the Greenland abrupt warming events suggests an oceanic transfer of the climate signal from the northern to the Southern Hemisphere. In contrast, an immediate response in Dx suggests an atmospheric teleconnection for example by a shift in the Intertropical Convergence Zone (ITCZ) and the Southern Hemisphere westerly wind belt (Buizert et al., 2018; Markle et al.,

2016), which is also observed in coupled climate models (Pedro et al., 2018).

All of these studies attest to the need for the best possible bipolar synchronization to get robust estimates of leads and lags as well as inferring the timescales of climate change. In Svensson et al. (2020) (referred to as S2020) the period 12–60 ka was matched by identification of volcanic eruptions in Greenland and Antarctic ice cores with a gap during the 16.5–24.5 ka period where high dust levels and small annual layer thickness complicate the bipolar matching. Here, we update and extend the bipolar volcanic matching to cover the entire 10–110 ka period providing a complete record of global climate phasing of the last glacial period. The new volcanic matching allows us to reveal the phasing of the climate signal in the two hemispheres at the D-O warming and cooling transitions with very high temporal precision. All reported ages are on the GICC05modelext time scale (Wolff et al., 2010) using the year 2000 CE as datum ('b2k' notation) unless otherwise stated.

2. Materials and methods

In this study, we apply records from the Greenland NGRIP, GRIP, GISP2 and NEEM ice cores, and from the Antarctic EDML, EDC, Dome Fuji (DF), TALDICE (TAL) and WD ice cores (see Table S0). The time scales of these ice cores are synchronized by identification of large volcanic acidity deposition events that are present in several or all of the cores. For the bipolar synchronization, NGRIP and EDML are used as master records in which all bipolar match points have been identified. The other cores are then matched up to NGRIP or EDML whenever possible. The applied records and their references are specified in Table S5.

All of the Greenland ice cores continuously cover the investigated period (10–110 ka), except for the interval 105–110 ka that is only covered by NGRIP and NEEM. NGRIP is the only record that preserves an annual resolution at the centimeter scale throughout the last glacial period. This is due to the basal melt occurring at this site, which reduces flow-based layer thinning in the deeper part of the record (North Greenland Ice Core Project members, 2004). The other applied Greenland cores are frozen to bedrock and have extensive thinning and folding of the deepest layers.

The Greenland ice-core time scales are synchronized (internally) using mostly existing electrical conductivity measurements (ECM) and dielectric profiling (DEP) based match points (Rasmussen et al., 2013;

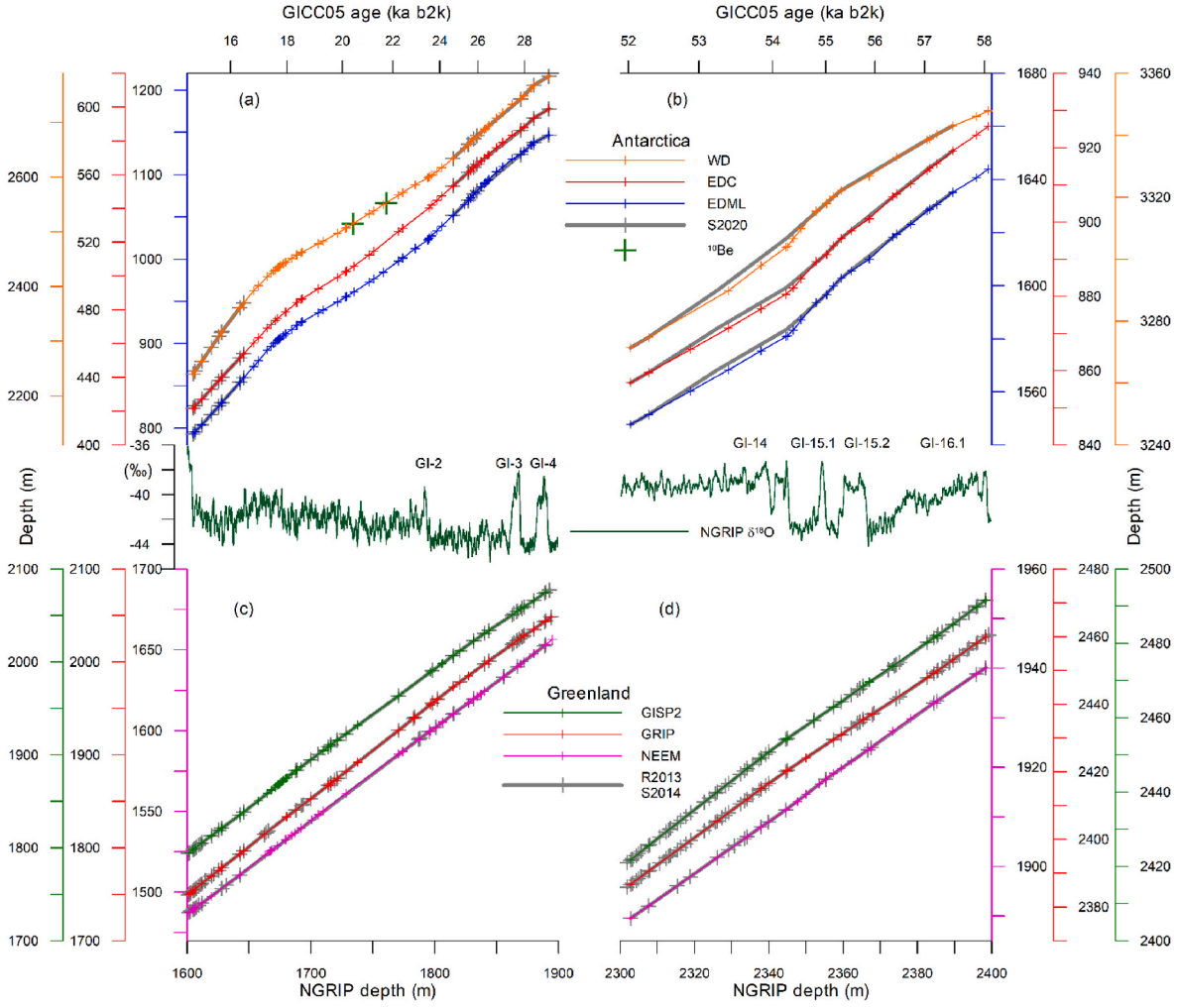

Fig. 1. Ice-core depth-depth relations between Greenland and Antarctica (a, b) and within Greenland (c, d) for selected periods. Small colored crosses show the depth of identified volcanic match points in this study and grey crosses show the depth of match points identified in previous studies. (a) and (c) show the age interval from GI-1 to GI-4 for which the 16.5–24.5 ka interval is matched up by volcanic matching for the first time. In (a) the large green crosses show the position of the bipolar NGRIP-WD ^{10}Be synchronization of Sinnl et al. (2023), and grey curves show the bipolar volcanic matching of S2020. (b) and (d) show the age interval 52–58 ka for which the bipolar volcanic matching is revised compared to that of S2020. In (b), colored curves show the present matching and grey curves show the matching of S2020. In (c) and (d) colored curves show the Greenland matching of this work whereas grey curves show the Greenland matching of Seierstad et al. (2014) (S2014 for GRIP and GISP2) and Rasmussen et al. (2013) (R2013 for NEEM). The middle panels show the NGRIP δ^{18}O record for reference.

Seierstad et al., 2014), but here additional match points are included applying continuous flow analysis (CFA) records that were unavailable at the time, thereby improving the overall match-point density. The new match points are in agreement with those published (Fig. 1c+d), except for the matching of the NEEM ice core in GS-19.2 (Fig. 2c) and for ice older than 95 ka (in GI-23, Fig. 2d). The matching of the GISP2 ice-core time scale has been improved during the last glacial maximum (LGM) from 17.2 to 18.4 ka and in the interval from GI-5.2 to GI-12 by applying a new high-resolution sulfur record (Table S5). Due to the lack of common volcanic fingerprints around GI-18 in the Greenland ice cores, the large increase in calcium concentration associated with the GI-18 warming transition in all Greenland cores has been used for the Greenland synchronization here (Rasmussen et al., 2014).

The EDML, EDC and DF ice cores continuously cover the entire investigated period whereas WD covers the period 10–67 ka and TAL is applied for the 10–61 ka interval below which the temporal resolution is very low and insufficient for precise synchronization. The records with highest temporal resolution are WD and EDML in the younger and older half of the last glacial period, respectively, due to their relatively high snow accumulation rates. On the other hand, the EDC and DF ice cores have rather constant temporal resolution in the 10–110 ka interval due to the lower accumulation and the location of the ice from the last glacial period in the upper (weakly thinned) part of the ice sheet at those locations.

The Antarctic EDML, EDC and WD ice cores have been synchronized internally in the last glacial period by identification of common acidity match points (Buizert et al., 2018; Ruth et al., 2007; Severi et al., 2007; Veres et al., 2013). Additional match points between EDML, EDC and WD have been introduced in this study in order to increase the match-point density and improve the matching precision. The internal Antarctic synchronization is important for periods where past accumulation patterns changed in different ways at the drilling locations, for example between West and East Antarctica towards the end of the last glacial period (WAIS Divide Project Members, 2013). For the linking of the DF and TAL ice cores, existing synchronizations have been applied (Buizert et al., 2018; Fujita et al., 2015; Oyabu et al., 2022; Severi et al., 2012) and additional EDML-DF match points have been introduced. All EDC depths reported here are on the EDC99 depth scale (Parrenin et al., 2012).

2.1. Bipolar linking methods

A first step in obtaining the bipolar synchronization is to establish an approximate bipolar depth-depth relation. This can be obtained from

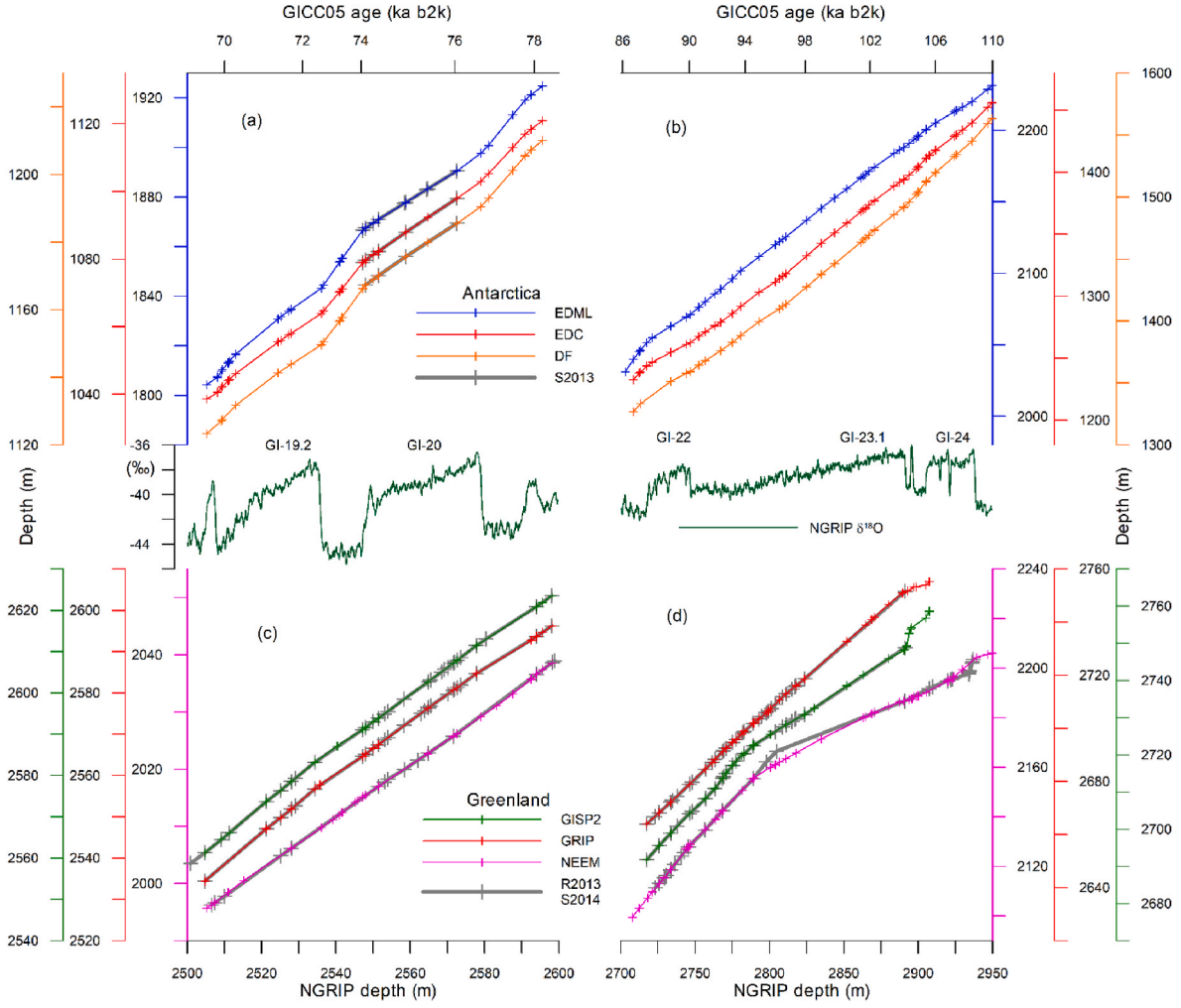

Fig. 2. Ice-core depth-depth relations between Greenland and Antarctica (a, b) and within Greenland (c, d) of selected periods. Small colored crosses show the depth of identified volcanic match points in this study and grey crosses show the depth of match points identified in previous studies. (a) and (c) show the age interval covering the major GI-19.2 and GI-20 events. In (a) grey curves show the bipolar volcanic matching of Svensson et al. (2013), related to the Toba 74 ka super eruption. (b) and (d) show the oldest section of the bipolar synchronization, 86–110 ka. In (c) and (d) colored curves show the Greenland matching of this work whereas grey curves show the Greenland matching of Seierstad et al. (2014) (S2014 for GRIP and GISP2), and Rasmussen et al. (2013) (R2013 for NEEM). The middle panels show the NGRIP $\delta^{18}O$ record for reference.

existing synchronizations based on gasses, cosmogenic isotopes or volcanoes, or from 'wiggle matching' at abrupt climate transitions assuming the bipolar seesaw pattern in the early last glacial is similar to that of the late glacial where a bipolar synchronization is established. The next step is then to fine-tune the synchronization by identifying identical patterns of volcanic eruptions in both Greenland and Antarctica. This is an iterative process, where different potential matches are tested for consistency with the methods discussed in the following sections.

2.1.1. Depth-depth relations among all cores

Compared to the study of S2020, where the main bipolar synchronization approach was parallel annual layer counting between match points in NGRIP and EDML, the approach in this study is different, because annual layers are too thin to be counted reliably in the deepest ice and over longer sections. Here the bipolar synchronization is to a higher degree based on the Greenland-Antarctic depth-depth relation inferred from the suggested bipolar match points of the ice cores (Fig. 1 + 2). The method is similar to that used to synchronize ice cores within Greenland (Seierstad et al., 2014) and within Antarctica (Severi et al., 2007). Between Greenland ice cores, the depth-depth relationship is generally a smooth function (Fig. 1c + d), because accumulation patterns change simultaneously over Greenland in a consistent manner and because ice-core thinning functions vary slowly with depth except in the very deepest ice-core sections (Fig. 2d). The same is to some extent true for Antarctic ice cores although their greater distance of separation (e.g. between East and West Antarctica and between coastal and central regions) leads to relative accumulation differences that give rise to larger variations in the depth-depth relationships (Fig. 1a). For the case of bipolar ice-core matching, depth-depth relations will show 'kinks' at depths of abrupt climate change in Greenland, such as the D-O warming and cooling transitions. At the D-O warming transitions, Greenland accumulation is known to increase abruptly by approximately a factor of two whereas the change in Antarctic accumulation is much smaller and more gradual (Bouchet et al., 2023). This gives rise to a characteristic zig-zag shape of the bipolar depth-depth relation across the GI-events (Fig. 2a). Because the kinks are a characteristic feature across GI events, the interpolar depth-depth relation can be applied to constrain suggested bipolar match points. In the deepest section of the ice cores, the thinning function typically is no longer smooth or even monotonous for ice cores that are frozen to bedrock or that have experienced folding. For this reason, the smooth depth-depth relation is interrupted for GRIP, GISP2 and NEEM in the earliest part of the last glacial (Fig. 2d).

2.1.2. Annual layer counting

Whenever possible, the bipolar matching is supported by annual layer counting in the NGRIP, EDML and/or WD ice cores as was done for S2020. This approach works when the high-resolution visual stratigraphy, dust or chemistry records resolve the annual layering between identified bipolar match points. The approach is generally not feasible across longer sections of Greenland stadial periods older than 60 ka, where the annual layer thickness are less than 1 cm. Annual layer counting in those sections may still be possible if analytical methods are optimized to resolve thin annual layers, such as was done for GS-22, 84.5–88.0 ka (Vallelonga et al., 2012), and for short intervals in the early last glacial and last interglacial periods (Svensson et al., 2011). Over longer intervals in the early glacial period, the depth-depth relation method outlined above is, however, a more robust approach than the annual layer counting that has typical uncertainties of 5 % (Svensson et al., 2008). In this study, annual layer counting has been applied between closely spaced bipolar match points to support the matching and around the D-O warming and cooling transitions in order to improve the bipolar synchronization of abrupt climate change events, but no continuous annual-layer counted time scale has been produced for the matched intervals.

2.1.3. ^{10}Be concentrations/fluxes

High-resolution continuous records of cosmogenic radionuclides such as ^{10}Be or ^{36}Cl, primarily reflecting geomagnetic and solar activity variations, provide another means of synchronizing ice cores between the two hemispheres. We performed a bipolar matching of selected sections using ^{10}Be records from GRIP (Muscheler et al., 2004; Wagner et al., 2001; Yiou et al., 1997) and EDML (Beer et al., 2025). The matching is challenging because there are few significant features to be matched at the resolution of the ^{10}Be records and because the volcanic matching of the GRIP record to the other Greenland ice cores is rather sporadic over longer sections of the early last glacial (Seierstad et al., 2014). Furthermore, additional noise is introduced into the ^{10}Be record by deposition processes, where the low glacial/stadial accumulation rates lead to a reduced dilution of dry-deposited aerosol compared to interglacial/interstadial conditions and, thus, we observe climate-related changes in the ^{10}Be concentration that are difficult to correct for accurately. Nevertheless, the bipolar ^{10}Be matching approach led to the discovery of an erroneous bipolar volcanic match in the 53–56 ka section that was published in S2020 and that is revised in the present work (see results section).

2.1.4. Tephra in bipolar sulfate spikes

The identified bipolar match points are checked against identified tephra deposits in the ice cores. The majority of ice-core tephra deposits are related to regional volcanic eruptions, making them less likely to have a bipolar imprint. For example, in Greenland most tephra deposits are of Icelandic origin (Abbott et al., 2012; Bourne et al., 2015; Cook et al., 2022), and the majority of those are associated with smaller-magnitude volcanic eruptions. The Antarctic WD match points have been screened for heavy metals that would support a regional volcanic source (Mason et al., 2022; Zreda-Gostynska et al., 1997). However, there are examples of very large eruptions with sulfate deposition at both poles that have deposited tephra at one pole. Examples of such eruptions are the Icelandic Vedde ash layer (12.2 ka), the Japanese Towada eruption (15.7 ka), the New Zealand Taupo eruption (25.5 ka) (those eruptions were included in the S2020 study), and the North Atlantic Ash Zone II (NAAZ II, 55.4 ka, see results section).

2.1.5. Bipolar methane matching

The bipolar volcanic matching has been applied to empirically determine the age difference between the ice and the encapsulated gas (Δage) in Antarctic ice cores (Buizert et al., 2021). In this study, the opposite approach was taken by applying the precise WD-GISP2 bipolar methane matching of Martin et al. (2023) to guide the search for a bipolar volcanic link in the period 16–20 ka. Informed by the bipolar gas matching and empirical estimates of GISP2 Δage, a bipolar match of closely spaced volcanic spikes was identified close to 18 ka which allowed a match across this section (Fig. 1a) where time scale synchronization has proven notoriously difficult both in Greenland (Seierstad et al., 2014) and between the hemispheres (S2020).

2.1.6. Stratospheric signature in sulfur isotopes

Since the identified bipolar sulfur depositions are generally not associated with tephra in the ice, there is a risk of identifying false positives of synchronously deposited sulfate at the two poles from regional volcanic eruptions that did not reach the stratosphere. From analyzing the sulfur isotopic composition of the ice-core sulfate it is, however, possible to determine whether the sulfate has been in the stratosphere via the mass-independent fractionation taking place there (Burke et al., 2019; Gautier et al., 2019; Savarino et al., 2003). This method can identify sulfate peaks that are due to regional volcanism if there is no stratospheric mass-independent fractionation sulfur isotopic signal. So far, ice-core sulfate isotope analyses have been carried out only for around 20 large glacial eruptions (Wolff et al., 2023), such as those associated with the Toba 74 ka eruption (Crick et al., 2021), but the method has potential to investigate the robustness of the bipolar

volcanic matching of the last glacial. All of the last-glacial global volcanic eruptions identified via sulfur isotopes are applied as bipolar volcanic match points in this study.

2.2. Identifying Greenland warming and cooling transitions

To investigate the bipolar phasing of climate variability around the Greenland abrupt D-O warming transitions from stadial to interstadial periods, a precise definition of the timing of those events is needed. We investigate the 33 major warming events as defined by Rasmussen et al. (2014) ranging from the Holocene onset to the warming related to the GI-24.2 onset.

The warming transitions are defined as the $\delta^{18}O$ transition mid-point in terms of amplitude, similar to the approach taken in WAIS Divide Project Members (2015) and S2020. Here, however, we apply the method to the average of the synchronized NGRIP, GRIP and NEEM $\delta^{18}O$ records, rather than the NGRIP record only, thereby reducing the $\delta^{18}O$ noise level. The GISP2 record is not included as it is measured at lower resolution (Table S4). To further reduce the noise, the averaged $\delta^{18}O$ record is smoothed by a 20-yr running mean for the mid-point determination. The identified NGRIP depths and ages of the warming transitions are mostly very similar to those applied in S2020, with an age difference of less than 10 years for 18 out of 21 transitions (Table S2). The exceptions to this are the warming transitions into the Holocene and into GI-13 and GI-15.2 that show an age difference of 15, 18, and 12 years, respectively.

The Greenland cooling transitions from interstadial to stadial periods are defined using a similar approach as the warming transitions using the average $\delta^{18}O$ of NGRIP, GRIP and NEEM. Because the cooling transitions are generally less abrupt than the warming transitions, they are more difficult to identify and there are larger differences to the transitions identified in S2020 based on NGRIP only (Table S3). Most notably, the Greenland cooling from GI-16.1 has been shifted by 144 yr towards younger ages.

2.3. CCSM4 model configuration

To compare with observations, we use the low-resolution version of the Community Climate System Model, version 4 (CCSM4) (Shields et al., 2012). The model couples atmosphere, ocean, land, and sea ice and is a computationally efficient alternative to the intermediate and standard resolution versions. This version of CCSM4 is ideally suited for long paleoclimate simulations. The model has an atmospheric horizontal grid of $3.75^\circ \times 3.75^\circ$ and includes 26 vertical levels with a spectral dynamical core (T31). The oceanic component of the model has a nominal 3° resolution (higher in the tropics) with 60 levels in the vertical. The T31x3 model has been validated for modern climate but has been modified to capture millennial-scale variability during the glacial period (see Vettoretti et al. (2022)). The model has slightly excessive Northern Hemisphere sea-ice extent and thickness, but generally simulates the modern climate with good fidelity. The model's representation of maximum zonal wind-stress magnitude in the Southern Hemisphere matches well with observational estimates over the ocean, and the model shows good agreement with observed variability, particularly for the El Niño-Southern Oscillation (ENSO). Surface-temperature anomaly trends for the twentieth century in the T31x3 model also align well with observations, but there is a general cold bias in the model. The glacial boundary conditions in Vettoretti et al. (2022) use ICE-6G (Peltier et al., 2015) ice-sheet reconstructions and orbital insolation for 21 ka BP. In Vettoretti et al. (2022) eight separate experiments were conducted with atmospheric CO_2 varying between 170 ppm and 240 ppm. Modifications were made to the ocean vertical mixing. In particular, the tidal mixing and overflow parameterizations were removed (as these are not known during the glacial period). A generic vertical mixing profile (Bryan and Lewis, 1979) from CCSM3 was used instead, and is crucial for the model to simulate D-O oscillations (Peltier and Vettoretti, 2014).

3. Results

In Table S1 the 300 bipolar volcanic match points obtained in this study and that of S2020 are listed together with five bipolar ^{10}Be match points related to the Laschamps geomagnetic excursion (Raisbeck et al., 2017). All of the match points are identified in the NGRIP and EDML cores that are the master records for the bipolar synchronization with their high-resolution sulfate concentration records. Whenever possible, the match points are also identified in the other cores. Despite the overall tight internal synchronization of the Greenland ice cores, only about half of the bipolar volcanic match points are identified in the NEEM, GRIP and GISP2 ice cores (56 %, 43 %, 53 %, respectively, Table S1 bottom). The Greenland synchronization is for a large part based on Icelandic volcanic reference horizons that are rarely present in Antarctica, and only NGRIP has high-resolution sulfate data, that most of the bipolar matching is based on, available across the full glacial period. The majority of the bipolar volcanic match points are identified in the EDC, WD (10–67 ka period only), DF and TAL (10–60 ka period only) ice cores (88 %, 95 %, 72 % and 68 %, respectively).

Fig. 3 shows the long-term bipolar climate evolution of the last glacial period along with the bipolar match points. It is noted that the match points are fairly evenly distributed over the investigated period with an average spacing of less than 330 yr (as compared to 500 yr for the S2020 study). Fig. 3 is expanded into the higher-resolution Figs. S01–S16 to provide more detail of the bipolar matching. Even more detailed zoom Figs. S17–S20 are provided for specific time intervals that have been synchronized for the first time in this work or that have been revised compared to the matching of S2020 (see discussion below.)

The matching of the 16.5–24.5 ka section has been a challenge. This is around the coldest part of the last glacial, referred to as the Last Glacial Maximum (LGM), where low snow accumulation probably results in poor sulfate-peak preservation in the ice cores. There is a reduced number of match points within Greenland (Seierstad et al., 2014), and the low annual-layer thickness limits the number of ice-core records with sufficient resolution to resolve the acidity peaks. Furthermore, the high dust content of the Greenland cores during the LGM mutes the acidity signal in the ECM records. The LGM volcanic matching was guided by the precise bipolar methane matching of Martin et al. (2023), and it is in agreement with the recent ^{10}Be bipolar match points between NGRIP and WD in GS-2, at circa 20.5 and 21.5 ka (Sinnl et al., 2023)(Fig. 1a). Fig. S17 shows a section of the LGM matching that covers the 192-yr long eruption of Mt. Takahe in West Antarctica (McConnell et al., 2017). This eruption is dominated by halogen emissions that are strongly reflected in the WD acidity profile and that will not have made it to Greenland.

The bipolar volcanic synchronization presented here includes the bipolar volcanic synchronization obtained for GI-20 including the period of the Toba 74 ka eruption, 74.0–76.5 ka (Lin et al., 2023; Svensson et al., 2013), except for minor adjustments. Twenty of the identified bipolar match points have been analyzed for sulfuric isotopic composition (Crick et al., 2021; Wolff et al., 2023), and they all show a stratospheric signature except for the 74.5 ka 'T4' Toba-related event (NGRIP depth 2551.45 m). The 'T4' event remains in the bipolar match-point list, however, as it is well constrained by annual layer counting and the bipolar depth-depth relation (Fig. 2).

For the first time, tephra from a large glacial volcanic eruption has now been identified in both Greenland and Antarctica. A limited number of micrometer-sized tephra grains from the Los Chocoyos (LCY) super-eruption from Atitlán Caldera in present-day Guatemala have recently been identified in the Greenland NEEM and the Antarctic EDC ice cores providing an independent bipolar tephra link (Innes et al., 2025). This exceptional tephra finding was made independently from the work presented here and the tephra confirms the bipolar link of very significant acidity spikes identified in all investigated cores situated in GI-21.1 at 80.1 ka (NGRIP depth 2619.14 m).

Table S2 shows the ice-core depths corresponding to the Greenland

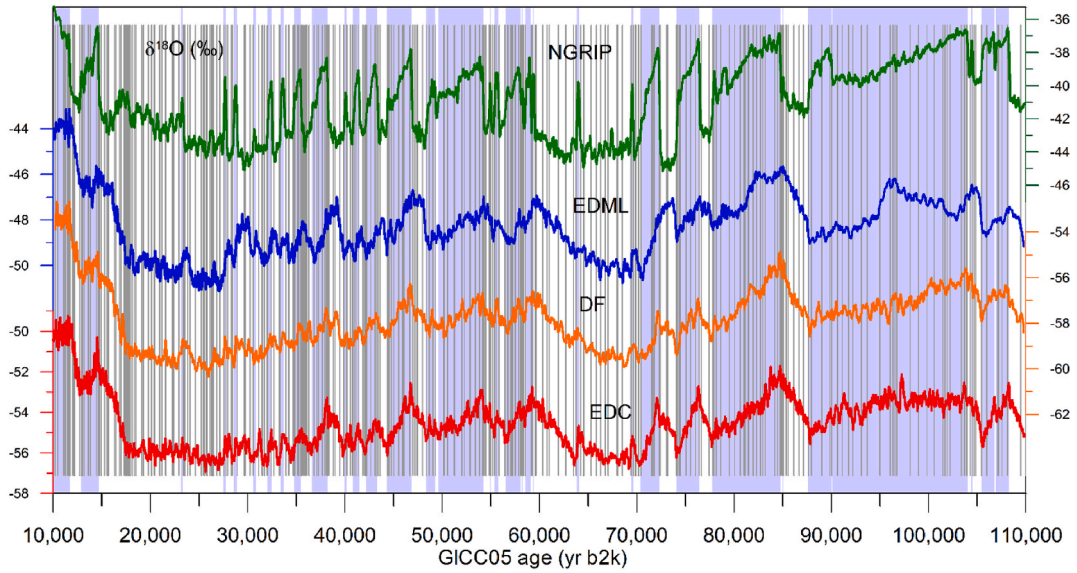

Fig. 3. Bipolar volcanic ice-core synchronization of Greenland (NGRIP) and Antarctic (EDML, DF, EDC) climate records ($\delta^{18}O$) at decadal-scale precision. Grey vertical lines are the identified global volcanic eruptions (Table S1). Purple-shaded intervals denote Greenland interstadial periods according to the definition of Rasmussen et al. (2014). The records are shown in higher temporal resolution in Figs. S01–S16.

D-O warming transitions in all investigated ice cores, as defined from the Greenland $\delta^{18}O$ warming transition midpoint (Methods), and Table S3 shows the depths corresponding to the Greenland D-O cooling transitions. The Antarctic depths are found by applying the bipolar volcanic synchronization between NGRIP and EDML and the volcanic synchronization of the Antarctic ice cores. The number of years between the nearest bipolar volcanic match point and the warming transition is denoted 'distance' in the table and the uncertainty of the bipolar transition matching is estimated to be 10 % of this number (denoted 'match uncertainty'). The 10 % combines an estimated 5 % counting uncertainty in both NGRIP and EDML as it was done for S2020. For most warming and cooling transitions this distance is less than 200 years. The distance is obtained from layer counting for transitions younger than 100 ka and from the modelled GICC05modelext and AICC2023 (Bouchet et al., 2023) time scales for transitions older than 100 ka.

3.1. *Changes made to the existing bipolar volcanic synchronization*

Since the publication of the bipolar volcanic match points for Marine Isotope Stages (MIS) 2 and 3 in S2020, some updates and revisions to the synchronization in this time period have been made. Some match points have been fine-tuned at the centimeter scale, and the higher density of bipolar match points in the present work has led to an increased precision of the bipolar synchronization. The change between the present study and that of S2020 in terms of shifts in NGRIP and EDML depths and ages at the abrupt Greenland transitions are indicated in Tables S2 and S3. For the Greenland cooling transitions most of the changes are related to the revised identifications of the midpoints of the Greenland $\delta^{18}O$ transitions.

For the Greenland warming transitions, the most important revisions of the bipolar matching have been made for the transitions into GI-5.1, GI-7, GI-11 and GI-14. At the GI-7 warming transition, the Antarctic cores have been shifted some 83 years towards older ages supported by 11 match points in the 34.5–36.5 ka interval (Figures S03, S13 and S18) compared to 3 match points over the same interval in the S2020 match (S2020 Fig. S6A + B). For the GI-5.1 and GI-11 warming transitions, an increased number of bipolar match points close to the transition is the reason for the shifts of 63 years towards older ages and 57 years toward younger ages, respectively.

For the GI-14 warming transition, an issue with the bipolar matching was first discovered for the construction of the DF2021 time scale, where the match led to inconsistent results of the Antarctic time scale (Oyabu et al., 2022). Subsequent comparison of ^{10}Be fluxes between Greenland (GRIP) and Antarctica (EDML) made it clear that the relative matching for the warming transitions into GI-14 as published by S2020 was offset by approximately 200 years with Antarctica being too young compared to Greenland. A revised synchronization with 12 bipolar match points has been obtained for the 53–56 ka interval (Figures S05, S15 and S19) as compared to 5 match points over the same interval for the S2020 match (S2020 Fig. S12A + B and S13A + B). A comparison of the ^{10}Be fluxes at the GRIP and EDML sites is shown in Fig. S21. In the revised version, the Antarctic counterpart to the GI-14 warming transition is shifted 152 yrs towards older ages (Fig. 1b). The warming transition of GI-14 is fixed by two volcanic events separated by 16 years that are clearly identified in both Greenland and Antarctica (Figure S19 and 54.2 ka).

4. Bipolar phasing of glacial climate

4.1. *Stacking of warming and cooling transitions*

With the purpose of investigating the more general bipolar climate pattern associated with the abrupt Greenland warming events, we investigate a stacked isotopic signal averaged over the D-O warming and cooling transitions (WAIS Divide Project Members, 2015; S2020). For both Greenland and Antarctic cores, the stacked isotopic signal is constructed by taking 1600 yr periods centered at the GI warming or cooling transition of each D-O cycle, aligning the individual events at the $\delta^{18}O$ transition midpoint, and subsequently averaging over the individual events to obtain the mean climatic response. For each event, the 1600 yr period is truncated in time to exclude neighboring events — i.e., if the stadial or interstadial periods on each side of the transition have a duration of less than 800 years. The truncation intervals of individual transitions are specified in Tables S2 and S3. The isotopic level of each event is shifted to a mean value of zero over the 1600 yr interval before truncation and averaging. The stack thus represents the isotopic anomaly across the transition rather than absolute values. This procedure is applied to both Greenland and Antarctic records. As specified in Table S4, the depth resolution of the $\delta^{18}O$ records vary from core to core and in some cases also with depth in the core.

Fig. 4 shows the stacked $\delta^{18}O$ records at the abrupt Greenland transitions for the NGRIP ice core and for each of the Antarctic ice cores. All the Antarctic stacked $\delta^{18}O$ signals except EDML show the same temporal pattern at the Greenland warming transitions (Fig. 4c). In accordance with the bipolar seesaw pattern, there is an Antarctic increase in $\delta^{18}O$ during the stadial periods that leads up to the Greenland warming. Thereafter, with the exception of EDML, a small abrupt warming occurs synchronously with the Greenland warming (Buizert et al., 2018). Importantly, in our improved synchronization the averaged Greenland warming reaches its maximum at 22 years (95 % confidence interval 16–27 years) and the averaged Antarctic warming reaches its maximum at 60 years (95 % confidence interval 39–146 years) after the midpoint of the Greenland warming (Fig. 5, Table S6). After the maximum, both Greenland and Antarctic records cool over the following centuries. The EDML stack shows a distinctly different behavior with the isotope signal showing a fairly constant level before the Greenland warming. At the time of the Greenland warming transition, the EDML record initiates a gradual cooling trend that lasts for several centuries. This Antarctic $\delta^{18}O$ response is qualitatively similar to that described by Buizert et al. (2018) based on bipolar methane synchronization, and by S2020 based on an earlier bipolar volcanic synchronization (Fig. 6). However, in the new synchronization the abrupt and immediate warming response is more pronounced. It has a larger magnitude, is spatially more widespread, and is now also clearly visible in the Antarctic-mean response.

Fig. S22 shows the Antarctic $\delta^{18}O$ signal related to the D-O warming transitions separated into stacks of 'major' and 'minor' events as defined in Table S4. 'Major events' refers to the 12 most significant Greenland warming events, and 'minor events' are the remaining 21 events. The major GI-transitions include those following Heinrich stadials in MIS 3 (GI-1, GI-2, GI-4, GI-8, GI-12, GI-14, GI-17.2) and those associated with longer interstadials in the early glacial (GI-19.2, GI-20, GI-21.1, GI-23.1, GI-24.2). Generally, the Antarctic peak following the Greenland warming transition has larger amplitude for the major events than for the minor events, and for the DF core this difference is very pronounced.

Similarly, Fig. S23 shows the Antarctic $\delta^{18}O$ signal related to the D-O warming transitions separated into stacks of 'younger' and 'older' events, where the age separation is at 65 ka. In general, the older events reach maximum warming sooner after the Greenland warming transition than the younger events. This is in accordance with the longer

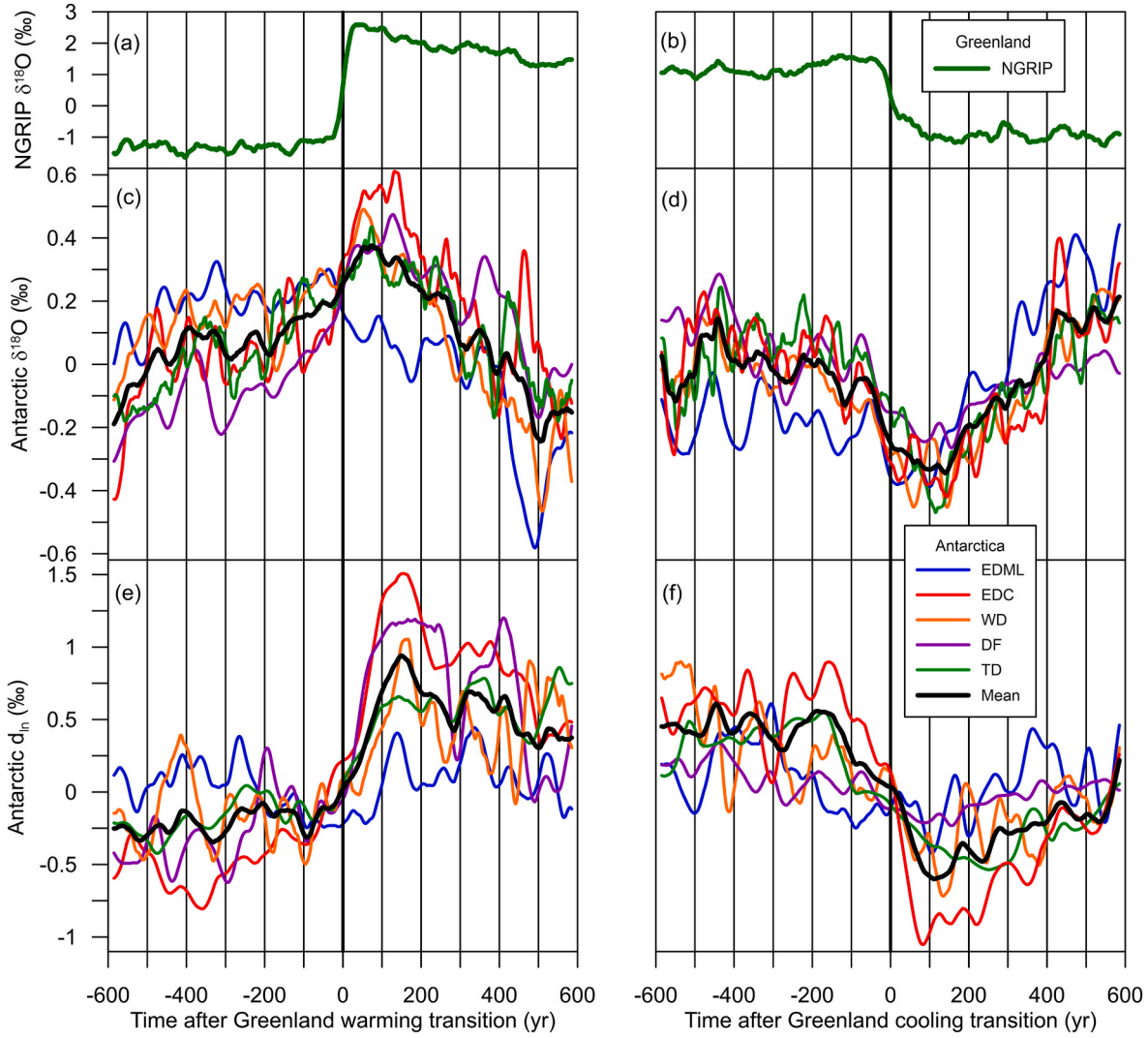

Fig. 4. Stacked Greenland (a–b) and Antarctic (c–f) water isotopic ice-core records across the Greenland warming (a,c,e) and cooling (b,d,f) transitions that occur at 't = 0'. (c–d) show stacks of $\delta^{18}O$ records for five individual ice cores (colors) as well as for the mean of the five (black), and (e–f) show the corresponding d_{ln} records. The number of events included for each core varies and is specified in Table S4. A 30-yr running mean has been applied to all shown records for clarity.

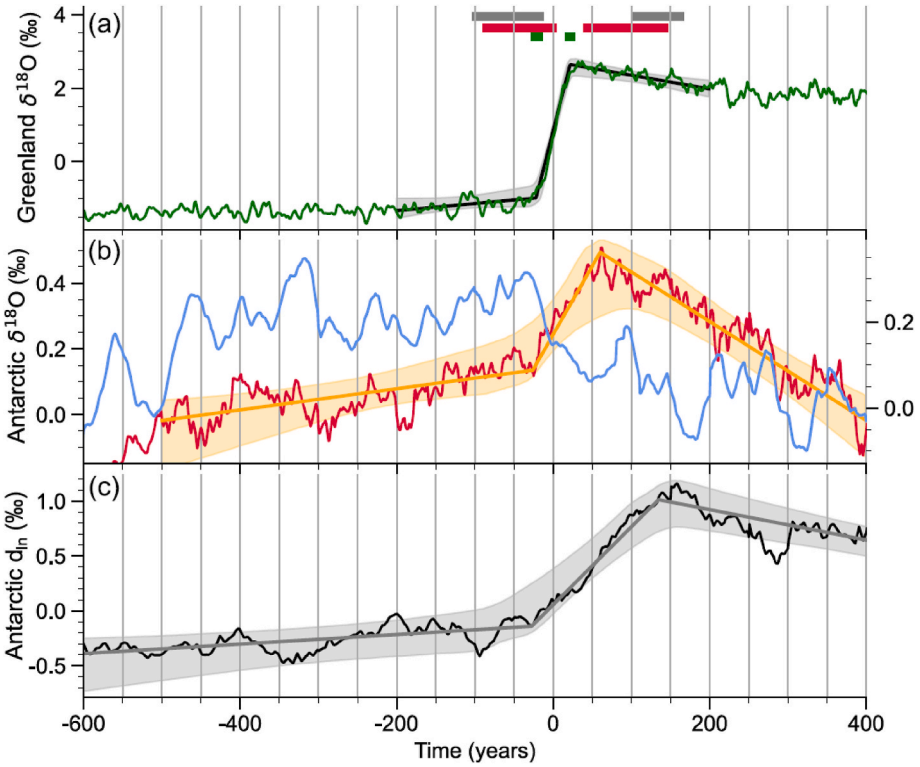

Fig. 5. Piecewise linear fit to the stacked ice-core records across the D-O warming transitions (same records as in Fig. 4). It is assumed that the records consist of a non-stochastic trend that represents the large-scale climate dynamics associated with D-O events, plus a stochastic component that represents climatic and non-climatic short-term variability in the stacked proxy. The stochastic component is represented by an autoregressive process that is added to the trend. We use a variant of the Metropolis algorithm to perform Bayesian inference on the parameters of the fit function and the stochastic process (see Supplementary text for method description). The fit parameters and confidence intervals for the transition onsets, transition peaks and transition durations are provided in Table S6. (a) Stacked Greenland $\delta^{18}O$ record comprising the NGRIP, NEEM and GRIP records (green) with a piecewise linear fit with two breakpoints (black). (b) Stacked Antarctic $\delta^{18}O$ record of EDML (blue, y-axis on right hand side) and of EDC, TAL, WD, and DF (red, y-axis on left hand side) with a piecewise-linear fit with two break points (orange). (c) Same as (b) but for the d_{ln} stack (excluding EDML). The lower uncertainty in the Greenland maximum reflects the higher signal-to-noise ratio of the stacked record compared to Antarctic records, since the amplitude of the D-O $\delta^{18}O$ transition is less than one tenth in Antarctica compared to Greenland. Above the time series, the colored bars indicate the 90 % confidence intervals of the isotopic break points in Antarctica and Greenland as obtained from the fit.

Antarctic warming transition times identified in earlier studies concerned with younger events only (Buizert et al., 2018; S2020). Interestingly, the EDML record changes behavior over time: for the younger events, EDML shows a cooling at the time of the Greenland warming transition whereas for the older events EDML shows a warming at this time – though its magnitude is similar to that of the internal climate/-signal variability at the site, making it hard to draw a robust conclusion.

The reason for the deviating EDML pattern is not understood, but it is a local phenomenon as the same pattern is not seen at the DF site that is also located in the Queen Maud Land sector. We stress that DF is at much higher altitude and located more than 30° west of EDML. Thus, it is much less influenced by air masses originating from the Weddell Sea sector with permanent sea-ice cover also at present times. We therefore speculate that the EDML signal is related to the sea-ice extent and possibly polynya dynamics in the Weddell Sea being out of phase with the general Antarctic climate at the Antarctic Isotopic maxima, but other reasons may also be at play. For example, $\delta^{18}O$ may capture effects other than local site temperature. Much of the vapor in EDML precipitation is sourced from the South Atlantic north of the Antarctic Circumpolar Current. This region experiences abrupt sea surface temperature (SST) decrease during D-O warming, which increases the source-to-site temperature difference leading to isotopically more depleted precipitation at EDML even in the absence of site-temperature changes; however, DF also receives a substantial portion of its vapor from the South Atlantic, making this explanation less likely than the aforementioned local Weddell Sea effects. We furthermore speculate that the temporal development of the EDML record over the last glacial period (Fig. S23), and the emergence of the EDML $\delta^{18}O$ anomaly in the younger events (<65 ka) could be related to upstream effects, as EDML is not situated on a dome. The deeper and older EDML ice originates from locations in the direction of Dome Fuji with the ice from the last interglacial period originating from about 150 km upstream (Huybrechts et al., 2007). In comparison the DF – EDML distance is around 1300 km along the flow line.

The Antarctic stacks of d_{ln} records for the Greenland abrupt climate transitions are shown in Fig. 4e + f. For the WD, DF and TAL cores, d_{ln} data are only available for a subset of the abrupt climate transitions of the last glacial, and for TAL the resolution of d_{ln} is lower than that of $\delta^{18}O$ (see Table S4 for specifications). The d_{ln} parameter is a logarithmic variant of the deuterium excess parameter, introduced for Antarctica by Uemura et al. (2012), and applied in previous bipolar stacking exercises (Buizert et al., 2018; Markle et al., 2016; Svensson et al., 2020). For reference, the corresponding Deuterium excess (Dx) stacks are shown in Fig. S25.

At the Greenland warming transitions, all the Antarctic d_{ln} records show an abrupt increase starting close to the Greenland warming transition, with the duration of the transition lasting for about 160 years (Fig. 5c–Table S6), followed by a gradual decay occurring over several centuries. The EDML d_{ln} shows a weaker response to the Greenland warming compared to the other Antarctic records. For the average of the Antarctic d_{ln} records, the increase occurring after the Greenland warming reaches a maximum at around 135 yr and is thus less abrupt than the increase in the Antarctic $\delta^{18}O$. The observed d_{ln} response is again qualitatively similar to earlier work based on both methane and

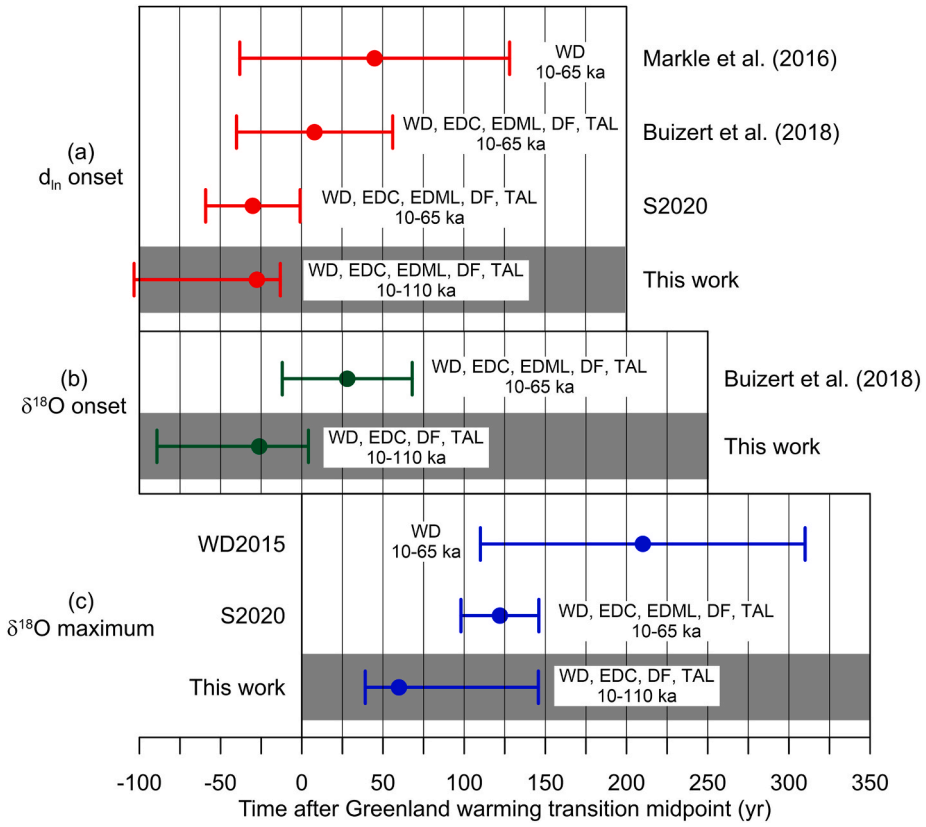

Fig. 6. Development of the timing of the 'Antarctic onset and delay' associated with the Greenland warming transitions. The dots show the timing of the average Antarctic d_{ln} (a) and $\delta^{18}O$ (b) onset and maxima (c) and their estimated time range relative to the Greenland warming transition midpoint occurring at 't = 0'. Results are shown for different studies that cover different ice cores and time intervals as indicated: WD2015; WAIS Divide Project Members (2015), S2020 (Svensson et al., 2020) and this study (Table S6).

volcanic bipolar synchronization (Buizert et al., 2018; Markle et al., 2016; S2020). Fig. S24 shows that the d_{ln} stacks for 'major' and 'minor' events are quite similar overall.

As mentioned, the Greenland cooling transitions related to D-O events are more difficult to pinpoint than the warming transitions and the stacks of the corresponding Antarctic isotope signal are therefore expected to be less well defined for the cooling events than for the warmings. Nevertheless, there is a clear change in both the Antarctic $\delta^{18}O$ and d_{ln} signals related to the Greenland cooling transitions (Fig. 4b + d + f).

Earlier work on bipolar phasing (Buizert et al., 2018; Svensson et al., 2020) derived a bipolar climate phasing for both the abrupt (atmospheric) mode, and the slower (oceanic) mode. Fig. 6 summarizes the evolution of these estimates over time, focusing on the D-O warming transitions. In the bipolar seesaw theory, the breakpoint in the Antarctic $\delta^{18}O$ time series going from a warming to a cooling trend is mechanistically linked to the abrupt warming transition in Greenland. Earlier work (WD2015, S2020) applied a line fitting algorithm with a single slope break to the Antarctic $\delta^{18}O$ stacks, which made sense in the absence of a clear abrupt $\delta^{18}O$ response. In the stacks presented here, to account for the abrupt $\delta^{18}O$ we instead apply a piece-wise linear fitting curve with two breakpoints (Fig. 5b), and interpret the peak $\delta^{18}O$ (or the second breakpoint) as the bipolar seesaw phasing in Antarctica. Over the last decade, estimates of the Antarctic time lag have decreased from 218 ± 100 years to our current estimated range of 39–146 years, with a best estimate of 60 years (Table S6). This trend reflects both the shift from bipolar methane synchronization to volcanic synchronization, as well as the inclusion of older (>65 ka) D-O events. We want to emphasize that all these times are relative to the Greenland D-O transition midpoint, chosen because its identification has the least degree of ambiguity. A dynamically more meaningful value for this delay would be derived from the onset of the Greenland D-O transition, which occurs at t = −26 years in our stacks (Table S6).

The phasing of the abrupt mode (suggested to reflect an atmospheric teleconnection) has been identified both through the onset of the d_{ln} response and through the onset of the abrupt component of the stacked Antarctic $\delta^{18}O$ signal. The inferred phasing of these elements has changed less over time (Fig. 6), though the general trend is likewise a shift toward earlier times such that the best estimates available now suggest that it is synchronous with the onset of the Greenland D-O transition in $\delta^{18}O$.

4.2. *Bipolar phasing in simulations of MIS 3 glacial climate*

We investigate bipolar phasing in four D-O oscillation simulations using the NCAR CCSM4 (Vettoretti et al., 2022), which exhibit regular and quasi-cyclic D-O cycles spanning a select range of constant atmospheric CO_2 levels (200, 210, 220, and 225 parts per million (ppm)) (see Fig. 7). For each of these CO_2 levels, the 8000-year long model simulations contain three to four simulated D-O warming events. Notably, simulated Greenland interstadials tend to last longer at higher CO_2 levels, while the stadials last for more extended periods at lower CO_2 concentrations, in agreement with observations (Buizert and Schmittner, 2015). Long interstadials in Greenland in the experiment with atmospheric [CO_2] at 225 ppm have a corresponding clearly visible cooling in Antarctica (Fig. 7a). Conversely, at lower CO_2 levels, Antarctic warming during steady, cool Greenland stadials exhibits an initial sharp increase, which then tapers off as the stadial progresses (Fig. 7d). This observed simulated behavior is consistent with that observed in the Stocker and Johnsen (2003) conceptual model of the bipolar seesaw,

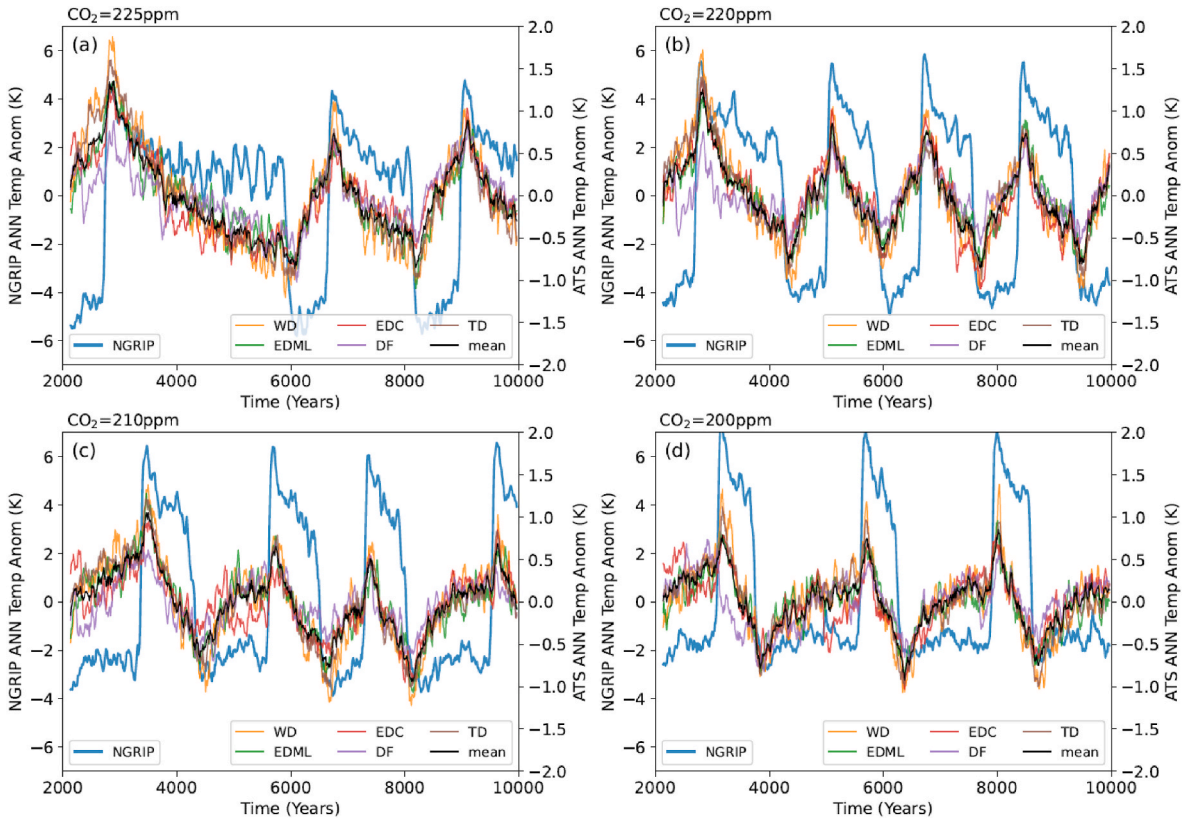

Fig. 7. Model 50-year running-mean temperature anomalies for NGRIP (blue) and the Antarctic Temperature Stack (ATS, black) and the individual locations (Wais Divide (WD, orange), EPICA Dome C (EDC, red), Taylor Dome (TD, brown), EPICA Dronning Maud Land (EDML, green), Dome Fuji (DF, purple)). The anomalies are relative to the average of each simulation. The simulations are for different constant background atmospheric CO_2 concentrations of a) 225 ppm, b) 220 ppm, c) 210 ppm, d) 200 ppm.

which exhibits a convolution of the Greenland temperature signal with an exponential factor expressed as a characteristic timescale. At intermediate CO_2 levels, the Antarctic cooling and warming phases appear more triangular, likely due to the shorter durations of both the interstadial and stadial stages (Capron et al., 2010a). In all simulated D-O Greenland warming events, a unique feature occurs over Antarctica at the abrupt warming in the Northern Hemisphere. Specifically, there is a noticeable change in the slope of stadial warming over Antarctica that corresponds precisely to the warming in Greenland. This pattern is particularly evident in the lower CO_2 simulations (Fig. 7c and d) and is consistent with the observed changes (Fig. 4).

The magnitude of the model-simulated stadial minimum to interstadial maximum in Greenland temperatures in the simulations is approximately 9 K, while those in Antarctica are about 1.5 K in magnitude, aligning well with temperature inferred from ice-core observations associated with warming events (e.g. Kindler et al. (2014)).

Rapid climatic anomalies near D-O warming events observed in both the model and the ice-core observations suggest the operation of an interhemispheric atmospheric teleconnection between the poles during Northern Hemisphere warming events. There is some indication that this also occurs during the transition from interstadial to stadial in the model (most clearly apparent in Fig. 7a and b).

We select twelve out of fourteen Greenland warming events from the four CCSM4 glacial simulations because the stacking analysis requires 600 years on either side of the D-O warming events. We then use this set of events to create a temperature stack in the same way as we did for the ice-core observations (Fig. 8a). The simulated temperatures from the core locations exhibit similar behavior across each of the model simulations, although this is not entirely consistent with ice-core observations. Specifically, the simulated stacked EDML temperature (Fig. 8a), looks like the simulated stacks for the other core locations, which is not the case for the EDML ice-core stack of $\delta^{18}O$ (Fig. 8b). This discrepancy could be due to several factors. One may be the model's inability to resolve and/or capture the correct changes in the extent of sea ice in the Weddell Sea. Other factors may be related to ocean−ice-shelf feedbacks that are not represented in the model, unaccounted temperature effects, incorrect moisture pathways and insufficient topographic resolution in this region. However, overall, the NGRIP and Antarctic temperature stacks appear very similar to the ice-core $\delta^{18}O$ stack. Both the observed ice-core stack and the simulated temperatures at the ice-core locations demonstrate minimal lag between the midpoint of Greenland warming and the peak of the Antarctic Isotope Maximum (AIM) in the Antarctic temperatures. In the simulation stack, the lag in the midpoint of the final increased gradient of warming in the Antarctic temperature signal, relative to the midpoint of the NGRIP warming event, is at most one to two decades. The model – data comparison becomes most convincing when only the 'major' ice-core warming events are compared to the model stack (Fig. 8c + d), suggesting that the model best captures this type of events. This may be a consequence of each model simulation using constant external and internal forcing, which prevents it from capturing the degree of signal variance seen in the ice-core data. The overall good agreement between model and observations strongly suggests that the model is capturing the global-scale dynamics associated with the Greenland warming events.

4.3. *Bipolar atmospheric and ocean teleconnections*

The role of the atmosphere and ocean in driving bipolar teleconnections between the poles is thought to involve several processes in the atmosphere and ocean on different timescales (see Buizert (2023) for an overview). For the oceanic connection, changes in the net transport of heat by the Atlantic between the southern and Northern Hemisphere is

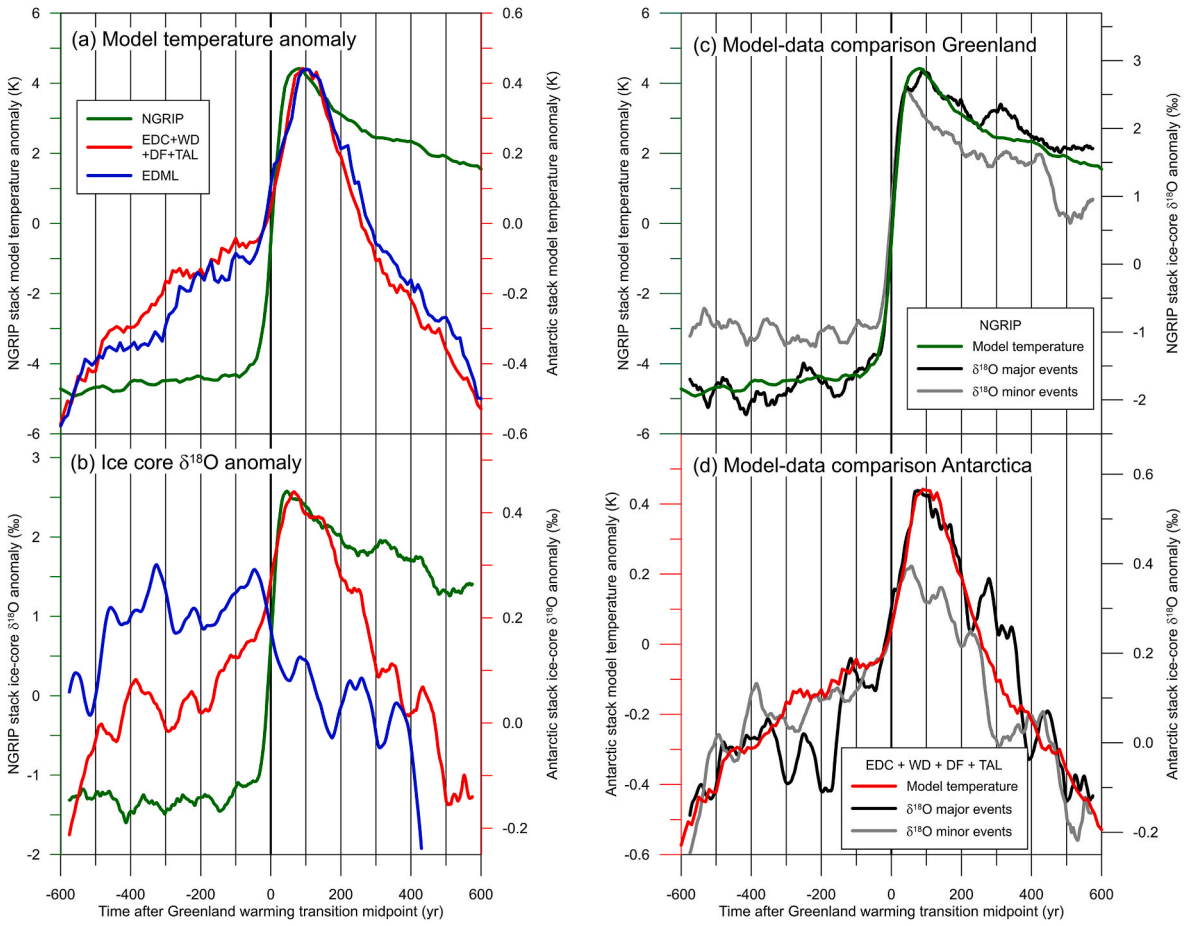

Fig. 8. Comparison of Greenland and Antarctic stacks of model temperature anomalies and ice-core $\delta^{18}O$ anomalies at the Greenland abrupt warming transitions. (a) shows a stack of modelled temperature records of 12 simulated D-O warming events out of the 4 simulations shown in Fig. 7. The Greenland NGRIP stack (green) and Antarctic stacks (red and blue) have the phasing set by the transition midpoint for each of the simulated NGRIP D-O warming events. The red curve shows the mean temperature at the four drilling locations. (b) shows stacked Greenland and Antarctic $\delta^{18}O$ ice-core records across the Greenland warming transitions (same records as in Fig. 4a + c). In (c) the stack of Greenland model temperature anomalies across the Greenland warming transitions is compared to the stack of Greenland NGRIP $\delta^{18}O$ anomalies divided into 'major' and 'minor' events as specified in Table S4. (d) shows the same as (c) but for Antarctic temperatures and $\delta^{18}O$ records. In figures (a) and (b), the green and red curves are scaled to have similar maxima and minima. In figures (c) and (d), the black and colored curves are scaled to have similar maxima and minima. A 50-yr running average has been applied to all shown records for clarity.

critical (Trenberth and Fasullo, 2017). During stadials, the AMOC transports less heat, and conversely more heat during interstadials (Pedro et al., 2018; Vettoretti and Peltier, 2018). A conceptual model of the bipolar seesaw with oceanic origins was presented by Stocker and Johnsen (2003) that convolves the Northern Hemisphere temperature signal with characteristic exponential timescale, thought to be approximately 1000 years (Buizert, 2023; Stocker and Johnsen, 2003).

A fast synchronous atmospheric signal between the poles has also been observed during D-O warming and cooling events (Buizert et al., 2018; Markle et al., 2016). From the proxy records of the ITCZ, the ITCZ and the associated precipitation bands shift to the warmer hemisphere during D-O warming events and southwards during cooling events (e.g. Ramirez et al. (2023)). The shifts are, however, not independent of the changes in ocean heat transport and AMOC strength as the position and strength of the Hadley cell are controlled by energetic constraints from the SSTs. Shifts in the ITCZ are thought to act in concert with shifts in the Southern Ocean winds. The southern eddy-driven jet is known to follow shifts in the ITCZ in modern climate (Ceppi et al., 2013), affecting the southern annular mode phase which is thought to be an important component in propagating changes to the high Southern latitudes during the glacial (Pedro et al., 2018).

In Fig. 9, we show a time sequence of a D-O warming event at model year 8000 from a simulation with a CO_2 concentration of 200 ppm. We investigate the anomalies from the mean climatology spanning 100 years surrounding the simulated D-O warming event. We focus on the zonally-averaged global ocean and zonally-averaged global atmosphere. The zonal-mean ocean temperature (Fig. 9a) shows the typical thermocline structure which matches the density structure of the ocean. The water-mass properties of the ocean tend to follow adiabatic pathways on neutral density surfaces (Marshall and Speer, 2012) and therefore interhemispheric ocean teleconnections would require a transport of heat between hemispheres via ocean processes that are mostly adiabatic in nature. These include the effect of mesoscale eddies mixing heat and salt along neutral density surfaces. The time variation of the zonal ocean anomalies is shown in Fig. 9b–g, from 40 years before the mid-point of the NGRIP D-O warming event to 60 years after. During the late stadial period (Fig. 9b), the interior ocean is anomalously warm and a thermal reservoir is visibly present in the global southern oceans as seen in CCSM4 and other models (Kuniyoshi et al., 2022; Pedro et al., 2018). The reduced AMOC during the cold phase of the D-O cycle is one major component that is responsible for this increase in ocean heat content (OHC). There is an especially large amount of thermocline OHC in the subpolar North Atlantic at 60°N (Vettoretti and Peltier, 2016) which is a source of the initial warming at NGRIP during the D-O warming (the

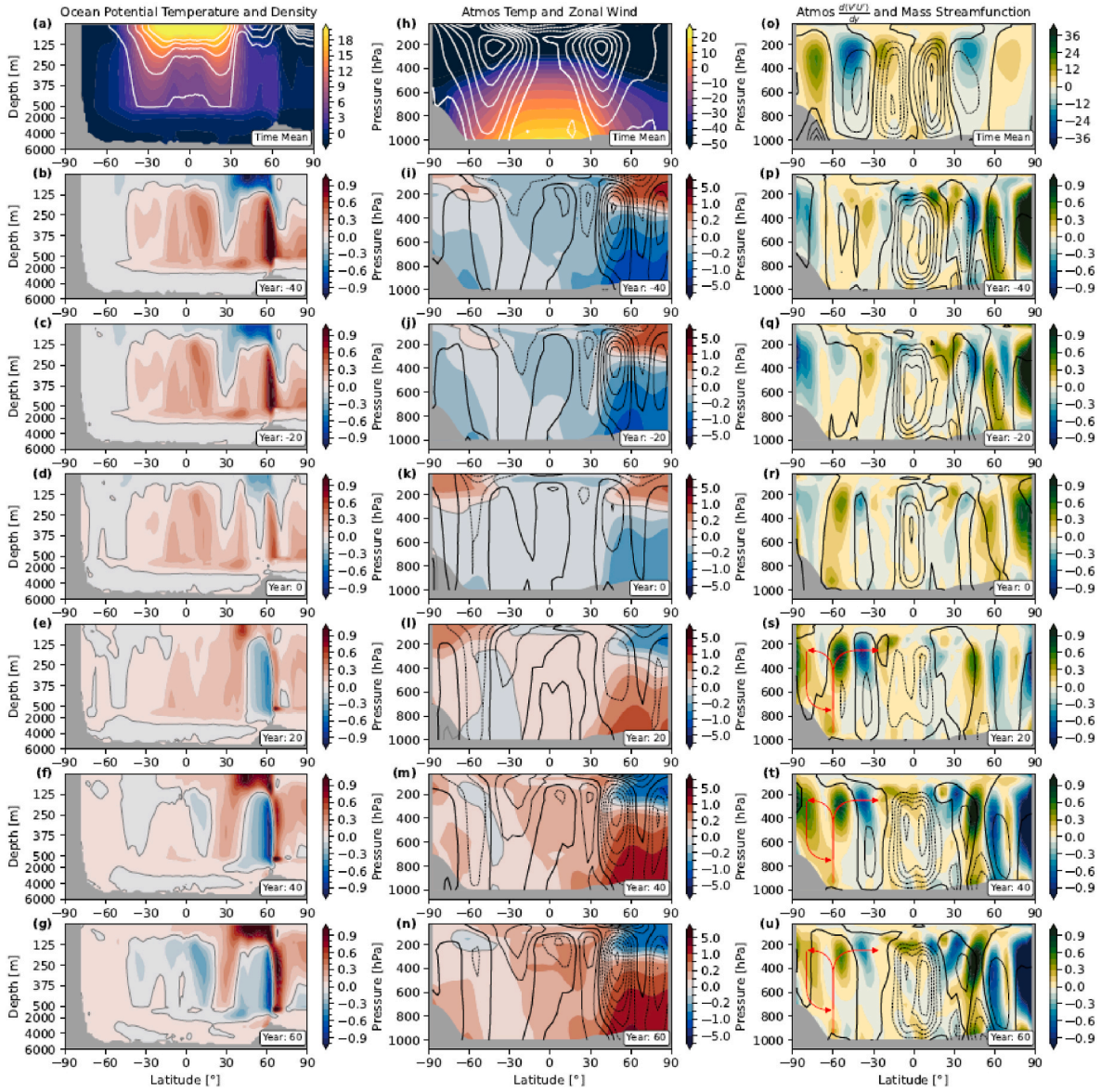

Fig. 9. a) Global zonally-averaged ocean temperature (shading) and potential density (contours) averaged over 100 years centered on the NGRIP D-O warming event at approximately year 8000 in Fig. 7d b-g) The temporal evolution of the zonally-averaged ocean-temperature anomalies relative to the 100-year average shown in a). h) The 100-year average global zonally-averaged atmospheric temperature (shading) and zonal winds (contours) as in a). i-n) The temporal evolution of the zonally-averaged atmospheric temperature and zonal wind anomalies relative to the 100-year average in h). o) Same as in h) but for the zonally-averaged latitudinal gradient in meridional eddy-momentum transport (shading) and mass stream function (contours). p-u) Same as in i-n) but for the temporal atmospheric anomalies from the 100-year average. Dashed lines are negative anomalies. The contour intervals are: zonal wind (20 m/s), zonal wind anomalies (0.2 m/s), mass stream function (20 m^2/s) and the mass stream function anomalies (1 m^2/s).

AMOC later contributes). The positive sub-surface anomaly in the mid-latitude Southern Ocean which reaches the glacial Southern Ocean sea-ice edge is thought to warm Antarctica during the stadial through radiative balance adjustments and atmospheric heat transport due to changes in sea-ice extent and albedo during the progression of the stadial (Pedro et al., 2018). During the Greenland warming transition (the 100-year period in Fig. 9b–g), the ocean gradually loses its heat content to the atmosphere, mostly in the North Atlantic and through northward transport by the AMOC. The loss of heat through the disappearance of sea ice in the North Atlantic is seen at 60°N as the warming event occurs (Fig. 9e). The reinvigoration of the AMOC and warmer North Atlantic Deep Water (NADW) production are visible as the warming event progresses (Fig. 9f and g).

The Southern Ocean mid-latitude thermocline (0–1000m depth) loses heat after the transition, which is consistent with longer timescale bipolar seesaw (Pedro et al., 2018). However, in this model, the ocean in higher southern latitudes (as well as over Antarctica) experiences a slight warming after the high northern latitude surface warming (Fig. 9e–g and 9l-n). Whether this ocean warming and atmospheric warming at high southern latitudes are connected is difficult to assess. It is unlikely that the temperature signal from the surface of Antarctica is subducted with deep water formation off the coast of Antarctica as the ocean has a much higher heat capacity and the signal would be damped. It is more likely that this observed high-southern-latitude ocean warming is associated with mixing and transport between mid-to-high southern latitudes from the Southern Ocean residual circulation which moves water masses counter clockwise at these latitudes. SH cooling is only visibly present in the simulations on the multi-decadal or centennial timescale well after the NGRIP warming event has occurred (Fig. 10). Ocean processes might be attributed as a fast teleconnection

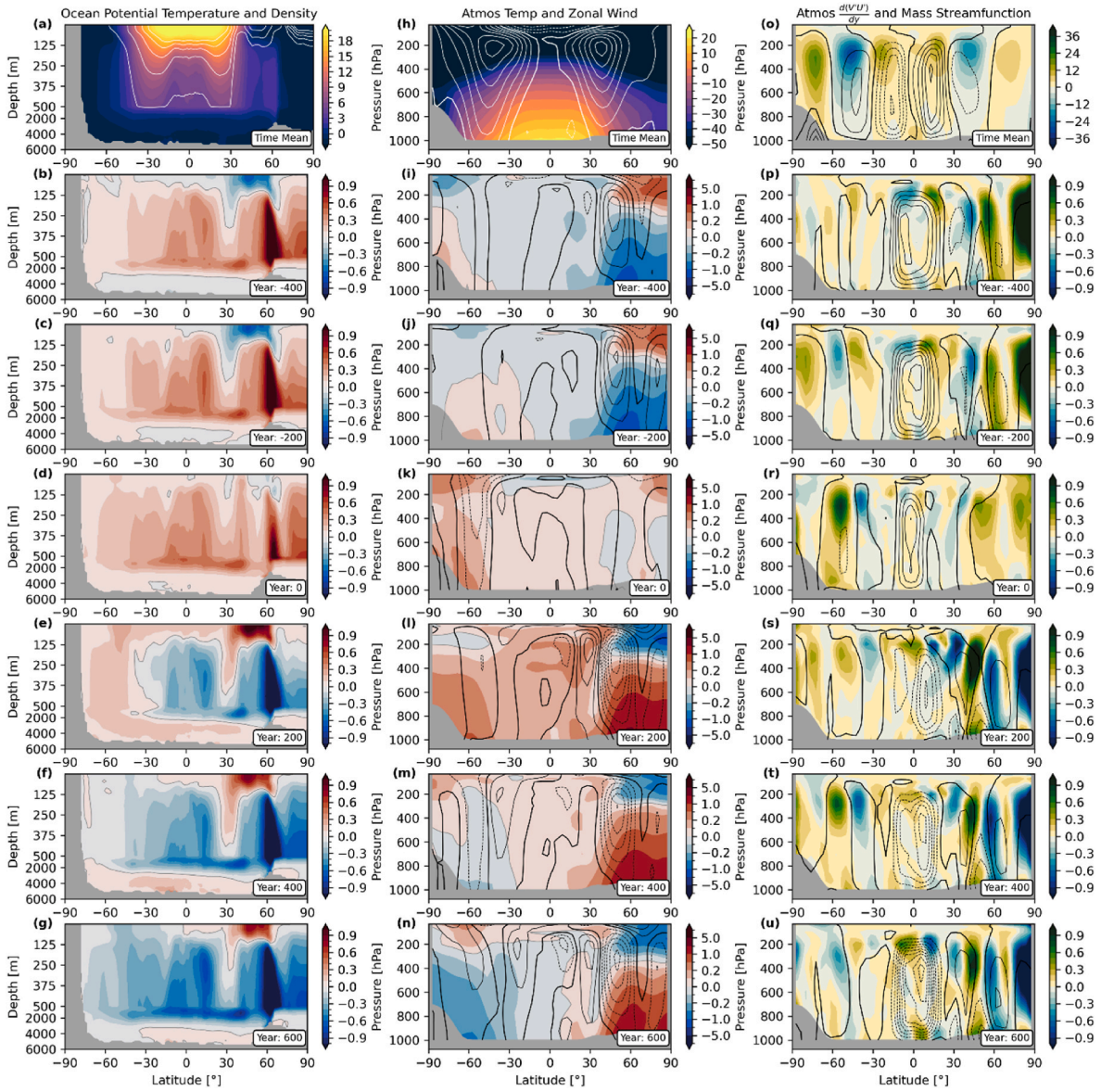

Fig. 10. Same as in Fig. 9 but for the time series spanning −400 years before the D-O warming event to +600 years after the event. Note that the Year 0 slice anomaly is different than in Fig. 9, because the anomaly is taken from a larger range of time (1000 years). The global ocean is shown but the Atlantic produces similar results with larger anomalies (See Figs. S28–S29).

mechanism for the large interhemispheric synchronous temperature signal observed in the bipolar ice-core synchronization presented here, but they would have to be transmitted by fast interhemispheric propagating coastally and equatorially trapped Kelvin waves (Johnson and Marshall, 2002). However, coarse ocean models, such as the one used in this study, may fail to support a coherent Kelvin wave mode, leading to spurious along-coast pressure variations and distorted phase velocities. Therefore we propose an explanation related to atmospheric dynamics.

Here we present an alternative scenario for an atmospheric mechanism to connect synchronous temperature signals between the poles that rests on atmospheric angular momentum balance, rather than on a meridional shift in the SH westerlies as proposed earlier-although a meridional shift in the SH westerlies does occur in these simulations.

This theory has been previously presented by Shin and Kang (2021) as a basis in understanding how high-latitude thermal forcing can affect the opposite hemisphere on a decadal timescale. Shin and Kang (2021) place part of the motivation of their study in a paleoclimate context to understand the bipolar seesaw, however they do not make the connection with the observed fast-timescale warming that we have shown here in the observations and model simulations.

Here we investigate if the fingerprints of this dynamical teleconnection operate in the glacial model simulations to explain the rapid synchronous temperature changes during a D-O warming event. The zonally-averaged atmospheric temperature (shading) and zonal wind (contours) over the 100-year period centered on the NGRIP D-O warming event is shown in Fig. 9h. Like the progression we see in the ocean anomalies, the zonally-averaged atmospheric temperature shows the clear switch from the Northern Hemisphere stadial conditions to interstadial conditions (Fig. 9i–n). During the late stadial (Fig. 9i), the Northern Hemisphere is cold in the troposphere and warm in the stratosphere. This effect is due to indirect effects where the increased water vapor in the upper troposphere/lower stratosphere due to warming increases longwave absorption, but the stratosphere trace gases continue to emit longwave radiation (Goessling and Bathiany, 2016). As the climate progresses toward the D-O warming transition, the Northern Hemisphere high-latitude troposphere warms (between 850 and 400 mb) and the Antarctic stratosphere also warms. As the warming event progresses (Fig. 9l–n), the positive temperature anomaly in the

northern high latitudes strengthens and appears to migrate equatorward and upwards towards the tropopause. Rather than the warming signal propagating at low levels, there is an atmospheric reorganization at high Southern latitudes over Antarctica. The atmosphere is reorganized with warm anomalous air mass descent over the South Pole and a cold anomalous ascent at southern mid-latitudes. By the end of the sequence, the atmosphere has established a pattern of both northern high-latitude warming and southern high-latitude warming. The stratospheric signal eventually synchronizes between the poles but appears slightly delayed compared with the tropospheric signal. The sequence of warming events suggests that the high-latitude atmospheric teleconnection is operating with a lag of a decade or two from the initial rapid warming observed at NGRIP in the climate model (Fig. 4a). The (Southern Hemisphere) zonal wind anomalies show slight equatorward migration of the combined subtropical and subpolar jet streams during the warming event. The Southern Hemisphere jets (Fig. 9h) are not separately resolved in the figure because of the zonal averaging and temporal smoothing (Fig. 9i–n).

The dynamical nature of the synchronous Antarctic warming requires further description. Fig. 9o shows the zonal mean mass transport (stream function, contours) by the atmosphere (Hadley, Ferrel and Polar cells) and the latitudinal convergence and divergence of eddy momentum covariance (shading). The zonally averaged eddy momentum covariance represents the areas of transport (positive northwards) where momentum is transported by eddies such as meridionally propagating Rossby waves or by atmospheric waves generated during baroclinic instability in midlatitude low-pressure systems. The poleward transport of eddy momentum is responsible for driving the sub-tropical zonal mean winds (eddy-driven jet) at altitude (Held and Hou, 1980). This positive convergence occurs in the upper atmosphere at the edges of the Hadley cell (where the Hadley cell descends). The Ferrel cell is mechanically driven by divergence of the eddy covariance as observed at mid-latitudes. The polar indirect cell is again in part a result of the eddy convergence. The stream function anomalies through the D-O warming event are characterized by a strengthening of the Southern Hemisphere Hadley cell and a weakening of the Northern Hemisphere Hadley cell (the negative anomalies from 20 ° S to 20° N in Fig. 9t and u). The anomalies in the eddy covariance convergence and divergence, that appear at elevation in the southern mid-to-high latitudes (Fig. 9r–u) after the warming event has started, are due to a shift in the southern subpolar and subtropical jets equatorward (Fig. 9i–n), a result of the strengthened Southern Hadley cell. The positive eddy anomaly at 55 ° S and negative anomaly at 40° S between 200 and 400 mb both contribute to an anomalous northward flow at altitude (see equation below).

The sequence of factors that result in the warming over Antarctica during the D-O warming event are as follows. The high-latitude lower-troposphere warming in the North Atlantic, sourced from the stored ocean heat, is spread hemispherically by the mean westerlies. The spreading to mid-latitudes is further propagated equatorwards by the lower branch of the Hadley cell and the extratropical trade winds (Shin et al., 2021). The northward surface direction of the lower branch of the Hadley cell south of the ITCZ causes a blocking effect. The warm anomalies rise to elevation in the tropics (Fig. 9l–n). With the ITCZ shifted northwards (Fig. S26) to the warmer hemisphere due to energetic constraints, the Southern Hemisphere branch of the Hadley cell increases in intensity (Fig. 9s–u) (Schneider et al., 2014). This strengthened Hadley cell south of the equator moves more equatorial angular momentum aloft and southwards ($\overline{vu}$), accelerating the southern sub-tropical jet (Ceppi et al., 2013; Held and Hou, 1980; Lindzen and Hou, 1988; Shin and Kang, 2021). Here $\overline{vu}$ is the mean meridional advection of mean angular momentum. A strengthened subtropical jet increases vertical wind shears through the thermal wind relation, increasing baroclinicity in the southern extratropics, moving the southern eddy-driven jet northwards (Lee and Kim, 2003). This equatorward shift induces anomalous eddy momentum convergence aloft at southern mid-latitudes and divergence poleward (Fig. 9s–u). The zonal momentum budget (Vallis, 2017) is

$$f\overline{v} \approx \frac{1}{a\,cos(\phi)} \frac{\partial(cos(\phi)\overline{v'u'})}{\partial y}.$$

Here u and v are the zonal and meridional wind respectively and a is the radius of the Earth. The overbars denote the zonal mean. Eddy (u, v) momentum convergence $\partial(u, v)/\partial y$ results in southward flow at the edge of the upper southern Hadley Cell and divergence results in northward flow at the upper southern Ferrel Cell ($f$the Coriolis parameter, is negative in the Southern Hemisphere) (Fig. 9o). The equatorward shifted eddy-driven jet due to the NGRIP D-O warming event results in anomalous northward flow aloft over the southern Ferrel and Hadley cells (Fig. 9s–u). This anomalous upper-level flow forces a counter-clockwise circulation over the Southern Ocean and Antarctica (red arrows in Fig. 9s–u). The descending motion over Antarctica adiabatically warms the South Polar troposphere (Shin and Kang 2021). The anomalous surface warming over Southern high latitudes then propagates equatorward. The motion in the southern mid-to-high latitudes resembles a "lava-lamp"-like indirect circulation (Fig. 9i–n). This overall adjustment of the atmosphere explains the rapid teleconnection seen between Greenland and Antarctica in both the ice cores and the climate model at the onset of a D-O warming event.

We want to emphasize that the mechanism we present here is not incompatible with the hypothesized shift in the SH westerlies proposed in earlier studies. Rather, it provides a mechanistic explanation for the observed abrupt warming signals over Antarctica. The proposed observational evidence for a shift in the SH westerlies during D-O variability is the Antarctic Dx signal, consistent with isotope-enabled climate model simulations that use the modern-day Southern Annular Mode as an analogue for such shifts in the past (Landais et al., 2021; Schmidt et al., 2007). How the mechanism by Shin and Kang (2021) impacts Antarctic isotope records of $\delta^{18}O$ and Dx is not known and should be investigated in subsequent work.

On a longer timescale the same diagnostics analysis presented above (Fig. 9) of the progression of the atmosphere and ocean anomalies before and after the D-O warming event is consistent with the theory of the bipolar seesaw in temperature that has been extensively documented in the literature (Fig. 10). In the centuries following a D-O warming event, when the Northern Hemisphere is warm, a strengthened AMOC enhances oceanic heat transport from the Southern Hemisphere to the Northern Hemisphere, leading to cooling in the Southern Ocean, a signature of the bipolar seesaw mechanism. This removal of heat from the Southern Ocean and global intermediate-depth oceans results in a series of knock-on effects. For example, the cooling over Antarctica in the centuries following the D-O event manifest itself through changes in surface radiation balance associated with increases in sea-ice albedo and extent. The southern surface ocean cools and the poleward atmospheric transport in the atmosphere transmits the signal over the Antarctic continent (Pedro et al., 2018).

In Fig. 10a–g, the zonal average global ocean displays this classic bipolar signal and is typical of that seen in other modelling simulations (Kuniyoshi et al., 2022; Pedro et al., 2018). The sequence of figures shows time steps of 200 years from 400 years before the D-O warming event to 600 years after the event. Note that the anomalies right at the D-O warming event are biased towards the 1200 year mean in the selected sequence (−600 to +600 years of the simulation surrounding the D-O event) and are mostly positive (Fig. 10d). However, 200 years after the warming event, the global ocean begins to cool in both the Southern and Northern Hemisphere. The Northern Hemisphere has a more pronounced cooling because the AMOC is in a strong state and the North Atlantic has released its anomalously warm subsurface heat to the atmosphere that was present before the onset of the D-O warming event. If the sequence of figures were continued, the Northern hemisphere cool ocean anomaly (in the Atlantic) would begin to warm as the AMOC weakens. While we show the Global Ocean anomalies here, the Atlantic Ocean anomalies shown in Figs. S28–S29, are of similar structure but are

of much greater amplitude, which highlights the role of the Atlantic in the bipolar seesaw.

The atmospheric zonal temperature anomalies (Fig. 10h–n) have an Antarctic temperature warm anomaly that peaks around 100 years after the D-O warming event (Fig. S27). The Southern Ocean cooling anomalies appear synchronous with the surface air temperature changes over Antarctica, as the bipolar seesaw establishes its characteristic pattern. We see also an anomalous northward migration of the Northern Hemisphere westerly jet (Fig. 10k–m). There is a slight equatorward shift in the Southern Hemisphere eddy-driven jet in the first 100 years following the D-O warming event (Ceppi et al., 2013; Shin and Kang, 2021). The anomalies in the convergence of eddy momentum flux over Antarctica and the Southern Polar Ocean appears to remain in place for up to 400 years after the D-O warming event at which point they begin to reverse (Fig. 10r–u). The strong impact from the cooling of the Southern Ocean likely dominates any downward adiabatic warming from the mechanism described above, but cooling over Antarctica may be slightly enhanced with this mechanism 600 years after the warming event with a reversal of the adiabatic decent changing to accent (Fig. 10u). The Hadley cell moves northward after the D-O warming event while the anomalous circulations in the Southern Hemisphere Ferrel cell appear to dissipate as the warming event progresses (Fig. 10r–u).

The phasing of atmospheric variables at specific latitudes and heights in the atmosphere are shown in Fig. 11. The warming at high northern latitudes shows the onset of the D-O warming event at 850 mb and 60°N (Fig. 11a). The corresponding warming over Antarctica at 850 mb and 75°S follows a similar pattern of warming at the D-O warming onset. The magnitude of the anomaly in the eddy momentum convergence corresponds to a generation of anomalous northerlies when the values go positive at the onset of the D-O event (see Shin and Kang (2021), Fig. 4). The Southern Hemisphere eddy-driven jet and Hadley Cell both show in-phase northward movement at the onset of the D-O warming event (Fig. 11b). However, both the Southern jet and eddy momentum convergence display a high degree of variability, so although the divergence of eddy momentum appears to lead the warming in the northern hemisphere, they may be synchronous.

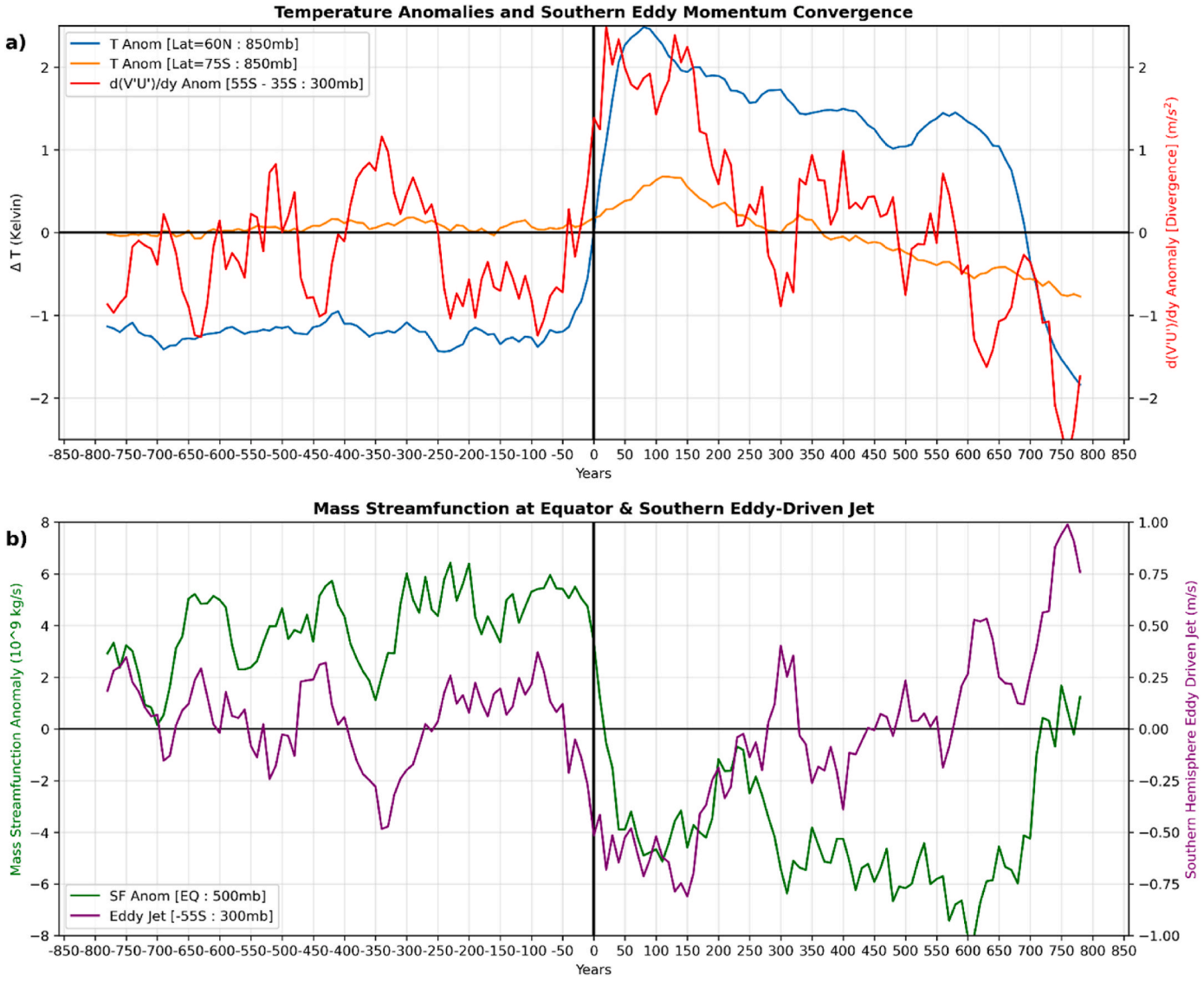

Fig. 11. a) The zonal average temperature anomalies at high northern (60°N) and southern latitudes (75°N) near the surface (850 mb) showing the D-O warming event (blue) in the north and the Antarctic warming (orange) in the south. The anomalous eddy momentum divergence (positive) induces anomalous upper level troposphere northerlies. b) The anomaly in the mass streamfunction at the equator and 500 mb (green) shows a northward migration of the Hadley Cell (and therefore ITCZ) when the streamfunction anomaly starts decreasing. The Southern Hemisphere eddy-driven jet is marked by anomalies in the zonal average winds at 55°S and 300 mb (purple).

5. Conclusions

A volcanic matching of Greenland and Antarctic ice cores has been generated for the last glacial period, 10–110 ka, by identification of 300 large volcanic eruptions with sulfate distribution in both Polar Regions. Together with five bipolar cosmogenic match points, the average spacing between match points of less than 330 years allows to determine the phasing of inter-hemispheric climate at decadal precision throughout the last glacial period.

On the centennial-to-millennial time scale, the bipolar climate phasing confirms the existence of an ocean-driven bipolar seesaw. The general behavior of the bipolar climate phasing associated with the abrupt Greenland climate transitions is investigated by stacking the climate record across all of the warming and cooling transitions of the last glacial. The stacking of the warming transitions shows a pattern where Greenland and Antarctica warm over a circa 22-yr and 60-yr long period, respectively, following the Greenland warming transition midpoint. The peak in Antarctic warmth lags the Greenland warming transition midpoint by 39–146 years (60 yr best estimate).

This pattern is seen in all the investigated Antarctic ice cores except the EDML core and it is consistent for both stronger and weaker Greenland warming transitions. At the EDML site located in the coastal Atlantic sector and receiving air masses from the Weddell Sea, a distinct pattern is observed in relation to the Greenland warming events in agreement with earlier studies. At EDML the stacked record shows a cooling (i.e., more negative $\delta^{18}O$) across the Greenland warming transition. The reason for this deviating pattern is not understood, but it is a local phenomenon as the same pattern is not seen at the DF site that is located on the boundary between the Atlantic and Indian Ocean sectors, but at higher elevation on the Antarctic plateau. The EDML exception requires further model and ice-core investigations in the future.

A comparison is made to a stack of unforced D-O-like oscillations generated by the NCAR CCSM4 model under MIS 3 climate conditions. The stacked ice-core data and model simulations show very comparable bipolar climate evolutions across the Greenland warming events in terms of timing and relative amplitudes suggesting that the model captures the main features of the events. However, the distinct behavior observed for the EDML site is not reproduced in the model as the model shows a climate pattern for EDML similar to that of the other modelled Antarctic ice-coring sites. Thus the climate model is not able to explain the EDML exception and lacks the feedbacks, mechanisms or resolution required to explain the Atlantic sector anomaly.

The climate model allows us to explore the dynamics of synchronous temperature changes during D-O warming events, where we focus on atmospheric teleconnections as observed in the glacial model simulations. The study reveals a distinct shift from Northern Hemisphere stadial to interstadial conditions and rapid corresponding atmospheric changes in the Southern Hemisphere. This pattern indicates a bipolar atmospheric teleconnection in the climate model. Notably, the warming sequence demonstrates a unique atmospheric reorganization, particularly over Antarctica, where warming occurs over Antarctica through adiabatic descent in the Southern polar latitudes as an indirect result of the abrupt D-O warming in the lower troposphere at high northern latitudes.

There are several applications of the bipolar volcanic matching presented here. One is for the construction of ice-core time scales that are consistent for Greenland and Antarctica (Bouchet et al., 2023; Oyabu et al., 2022). Because accumulation patterns change differently between Greenland and Antarctica, the bipolar synchronization provides tighter constraints for both modelled and layer-counted bipolar time scales compared to those based on ice cores from one Hemisphere only. It also refines the phasing between changes in temperatures and atmospheric gas concentrations as Δage is constrained by the bipolar matching (Buizert et al., 2021). Once the bipolar ice-core time scales are consistent, any paleo-information that can be linked to a polar ice core can be put in a global climatic context.

Another application of the bipolar volcanic matching is for the quantification and occurrence rate of last-glacial large volcanic eruptions (Lin et al., 2022). The bipolar linking allows us to discriminate large volcanic eruptions with stratospheric sulfate injection and global climatic impact from regional volcanism where sulfate is mostly transported in the troposphere. Because the ice cores provide continuous records of sulfate deposition, they offer more complete volcanic occurrence records than those obtained from geological approaches in a 100-ka time frame (e.g. Crosweller et al. (2012) and Schindlbeck-Belo et al. (2024)).

Author contributions

Anders Svensson has been leading the volcanic synchronization work.

Guido Vettoretti has carried out CCSM4 model simulations and led the discussion of the model dynamics interpretation.

Jia-mei Lin and Giulia Sinnl have contributed to the bipolar synchronization using both volcanic and cosmogenic stratigraphic markers.

Dorthe Dahl-Jensen, Jørgen Peder Steffensen, Sune Olander Rasmussen, and Bo Vinther have contributed with ice-core conductivity and water isotope datasets and been involved in the discussion and interpretation of results.

Christine Hvidberg has supervised on the implementation of ice core thinning models at the drill site locations.

Helle Astrid Kjær, Vasileios Gkinis, and Eliza Cook have contributed to the implementation of high-resolution chemistry, water isotope and tephra results for the bipolar synchronization.

Johannes Lohmann has made the fit functions for the abrupt warming transitions and contributed to the interpretation of those.

Jonathan Ortved Melcher and Sune Halkjær have contribution to the data-model comparison at the warming transitions.

Sepp Kipfstuhl and Frank Wilhelms have contributed with ice-core conductivity records and discussions and the interpretation of those and other ice-core records.

Florian Adolphi, Jürg Beer, and Raimund Muscheler have provided cosmogenic isotope records and applied those to test and improve the bipolar volcanic synchronization.

Hubertus Fischer has contributed to the production of continuous ice-core records and to the interpretation of results.

Matthias Bigler has had a key role in producing several of the applied high resolution data sets.

Michael Sigl has contributed to the bipolar matching from a tephra and acidity perspective.

Amaelle Landais, Marie Bouchet, Frederic Parrenin and Anna Klüssendorf have worked on ice core time scales and the exact bipolar phasing at the abrupt transitions.

Robert Mulvaney has provided insights to the use of the NEEM high resolution records.

Eric Wolff, Andrea Burke, Helen Innes, Mirko Severi have contributed with sulfate and tephra data sets and with the interpretation of those in a bipolar context.

Christo Buizert has written part of the manuscript and contributed to the bipolar linking and to the interpretation of results.

Joseph R. McConnell, Nathan Chellman and Sophia Wensman have provided the new GISP2 high resolution dataset.

Ikumi Oyabu has contributed to the synchronization of the Dome Fuji ice core to the other Antarctic cores.

Disclaimer

Views and opinions expressed are however those of the author(s) only and do not necessarily reflect those of the European Union or the European Research Council Executive Agency. Neither the European Union nor the granting authority can be held responsible for them.

Declaration of competing interest

The authors declare that they have no known competing financial interests or personal relationships that could have appeared to influence the work reported in this paper.

Acknowledgments

AS and DDJ were funded by the European Union (ERC, Green2Ice, 101072180). The Division for Climate and Environmental Physics of the Physics Institute, University of Bern, gratefully acknowledges the long-term support of Greenland and Antarctic ice-core research at the University of Bern by the Swiss National Science Foundation. EW was supported by a Royal Society Professorship. CB gratefully acknowledges funding from the US National Science Foundation (award 2315928). HAK was funded by the H2020 project TiPES (820970), H2020 project P2F (101184070) and the Danish DFF project (1131-00007B). We acknowledge US NSF awards 2102917 and 1702830 for GISP2 sulfur measurements contributed by JRM, NC, and SW. AB gratefully acknowledges funding from a Philip Leverhulme prize in Earth Sciences (PLP-2021-167). FP acknowledges the funding by CNR/INSU/LEFE for the IceChrono and CO2Role projects. M. Sigl received funding from the European Research Council under the European Union's Horizon 2020 research and innovation programme (grant number: 820047).

Appendix A. Supplementary data

Supplementary data to this article can be found online at https://doi.org/10.1016/j.quascirev.2025.109755.

Data availability

The datasets applied in this study are mostly already published. Table S6 provide references to the original publications.

References

Abbott, P.M., Davies, S.M., Steffensen, J.P., Pearce, N.J.G., Bigler, M., Johnsen, S.J., Seierstad, I.K., Svensson, A., Wastegard, S., 2012. A detailed framework of Marine Isotope Stages 4 and 5 volcanic events recorded in two Greenland ice-cores. Quat. Sci. Rev. 36, 59–77.

Beer, J., McCracken, K.G., Adolphi, F., Christl, M., Fischer, H., Miller, H., Muscheler, R., Synal, H.A., Wilhelms, F., 2025. Heliomagnetic and geomagnetic activity cycles on millennial timescales. Quat. Sci. Rev. 361.

Bender, M., Sowers, T., Dickson, M.-L., Orchardo, J., Grootes, P., Mayewski, P.A., Meese, D.A., 1994. Climate correlations between Greenland and Antarctica during the last 100,000 years. Nature 372, 663–666.

Blunier, T., Chappellaz, J., Schwander, J., Dällenbach, A., Stauffer, B., Stocker, T.F., Raynaud, D., Jouzel, J., Clausen, H.B., Hammer, C.U., Johnsen, S.J., 1998. Asynchrony of Antarctic and Greenland climate change during the last glacial period. Nature 394, 739–743.

Bouchet, M., Landais, A., Grisart, A., Parrenin, F., Prié, F., Jacob, R., Fourré, E., Capron, E., Raynaud, D., Lipenkov, V.Y., Loutre, M.F., Extier, T., Svensson, A., Legrain, E., Martinerie, P., Leuenberger, M., Jiang, W., Ritterbusch, F., Lu, Z.T., Yang, G.M., 2023. The Antarctic Ice Core Chronology 2023 (AICC2023) chronological framework and associated timescale for the European Project for Ice Coring in Antarctica (EPICA) Dome C ice core. Clim. Past 19, 2257–2286.

Bourne, A.J., Cook, E., Abbott, P.M., Seierstad, I.K., Steffensen, J.P., Svensson, A., Fischer, H., Schupbach, S., Davies, S.M., 2015. A tephra lattice for Greenland and a reconstruction of volcanic events spanning 25-45 ka b2k. Quat. Sci. Rev. 118, 122–141.

Bryan, K., Lewis, L.J., 1979. A water mass model of the World Ocean. J. Geophys. Res. 84, 2503.

Buizert, C., 2023. The thermal bipolar seesaw during abrupt climate change. Reference Module in Earth Systems and Environmental Sciences. Elsevier.

Buizert, C., Fudge, T.J., Roberts, W.H.G., Steig, E.J., Sherriff-Tadano, S., Ritz, C., Lefebvre, E., Edwards, J., Kawamura, K., Oyabu, I., Motoyama, H., Kahle, E.C., Jones, T.R., Abe-Ouchi, A., Obase, T., Martin, C., Corr, H., Severinghaus, J.P., Beaudette, R., Epifanio, J.A., Brook, E.J., Martin, K., Chappellaz, J., Aoki, S., Nakazawa, T., Sowers, T.A., Alley, R.B., Ahn, J., Sigl, M., Severi, M., Dunbar, N.W., Svensson, A., Fegyveresi, J.M., He, C., Liu, Z., Zhu, J., Otto-Bliesner, B.L., Lipenkov, V.Y., Kageyama, M., Schwander, J., 2021. Antarctic surface temperature and elevation during the Last Glacial Maximum. Science 372, 1097–1101.

Buizert, C., Schmittner, A., 2015. Southern Ocean control of glacial AMOC stability and Dansgaard-Oeschger interstadial duration. Paleoceanography 30, 1595–1612.

Buizert, C., Sigl, M., Severi, M., Markle, B.R., Wettstein, J.J., McConnell, J.R., Pedro, J.B., Sodemann, H., Goto-Azuma, K., Kawamura, K., Fujita, S., Motoyama, H., Hirabayashi, M., Uemura, R., Stenni, B., Parrenin, F., He, F., Fudge, T.J., Steig, E.J., 2018. Abrupt ice-age shifts in southern westerly winds and Antarctic climate forced from the north. Nature 563, 681–685.

Burke, A., Moore, K.A., Sigl, M., Nita, D.C., McConnell, J.R., Adkins, J.F., 2019. Stratospheric eruptions from tropical and extra-tropical volcanoes constrained using high-resolution sulfur isotopes in ice cores. Earth Planet Sci. Lett. 521, 113–119.

Capron, E., Landais, A., Chappellaz, J., Schilt, A., Buiron, D., Dahl-Jensen, D., Johnsen, S. J., Jouzel, J., Lemieux-Dudon, B., Loulergue, L., Leuenberger, M., Masson-Delmotte, V., Meyer, H., Oerter, H., Stenni, B., 2010a. Millennial and sub-millennial scale climatic variations recorded in polar ice cores over the last glacial period. Clim. Past 6, 345–365.

Capron, E., Landais, A., Lemieux-Dudon, B., Schilt, A., Masson-Delmotte, V., Buiron, D., Chappellaz, J., Dahl-Jensen, D., Johnsen, S., Leuenberger, M., Loulergue, L., Oerter, H., 2010b. Synchronising EDML and NorthGRIP ice cores using delta O-18 of atmospheric oxygen (delta O-18(atm)) and CH4 measurements over MIS5 (80-123 kyr). Quat. Sci. Rev. 29, 222–234.

Ceppi, P., Hwang, Y.T., Liu, X., Frierson, D.M.W., Hartmann, D.L., 2013. The relationship between the ITCZ and the Southern Hemispheric eddy-driven jet. J. Geophys. Res. Atmos. 118, 5136–5146.

Cook, E., Abbott, P.M., Pearce, N.J.G., Mojtabavi, S., Svensson, A., Bourne, A.J., Rasmussen, S.O., Seierstad, I.K., Vinther, B.M., Harrison, J., Street, E., Steffensen, J. P., Wilhelms, F., Davies, S.M., 2022. Volcanism and the Greenland ice cores: a new tephrochronological framework for the last glacial-interglacial transition (LGIT) based on cryptotephra deposits in three ice cores. Quat. Sci. Rev. 292.

Crick, L., Burke, A., Hutchison, W., Kohno, M., Moore, K.A., Savarino, J., Doyle, E.A., Mahony, S., Kipfstuhl, S., Rae, J.W.B., Steele, R.C.J., Sparks, R.S.J., Wolff, E.W., 2021. New insights into the ~ 74 ka Toba eruption from sulfur isotopes of polar ice cores. Clim. Past 17, 2119–2137.

Crosweller, H.S., Arora, B., Brown, S.K., Cottrell, E., Deligne, N.I., Guerrero, N.O., Hobbs, L., Kiyosugi, K., Loughlin, S.C., Lowndes, J., Nayembil, M., Siebert, L., Sparks, R.S.J., Takarada, S., Venzke, E., 2012. Global database on large magnitude explosive volcanic eruptions (LaMEVE). Journal of Applied Volcanology 1.

EPICA community members, 2006. One-to-one coupling of glacial climate variability in Greeland and Antartctica. Nature 444, 195–198.

Fujita, S., Parrenin, F., Severi, M., Motoyama, H., Wolff, E., 2015. Volcanic synchronization of Dome Fuji and Dome C Antarctic deep ice cores over the past 216 kyr. Clim. Past Discuss 11, 407–445.

Gautier, E., Savarino, J., Hoek, J., Erbland, J., Caillon, N., Hattori, S., Yoshida, N., Albalat, E., Albarede, F., Farquhar, J., 2019. 2600-years of stratospheric volcanism through sulfate isotopes. Nat. Commun. 10.

Goessling, H.F., Bathiany, S., 2016. Why CO_2 cools the middle atmosphere – a consolidating model perspective. Earth Syst. Dyn. 7, 697–715.

Held, I.M., Hou, A.Y., 1980. Nonlinear axially symmetric circulations in a nearly inviscid atmosphere. J. Atmos. Sci. 37, 515–533.

Huybrechts, P., Rybak, O., Pattyn, F., Ruth, U., Steinhage, D., 2007. Ice thinning, upstream advection, and non-climatic biases for the upper 89% of the EDML ice core from a nested model of the Antarctic ice sheet. Clim. Past 3, 577–589.

Innes, H.M., Hutchison, W., Sigl, M., Crick, L., Abbott, P.M., Bigler, M., Chellman, N.J., Davies, S.M., Kutterolf, S., McConnell, J.R., Severi, M., Sparks, R.S.J., Svensson, A., Wolff, E.W., Rae, J.W.B., Burke, A., 2025. Ice core evidence for the Los Chocoyos supereruption disputes millennial-scale climate impact. Commun. Earth Environ. 6, 137.

Johnson, H.L., Marshall, D.P., 2002. A theory for the surface atlantic response to thermohaline vairability. J. Phys. Oceanogr. 32, 1121–1132.

Kindler, P., Guillevic, M., Baumgartner, M., Schwander, J., Landais, A., Leuenberger, M., 2014. Temperature reconstruction from 10 to 120 kyr b2k from the NGRIP ice core. Clim. Past 10, 887–902.

Kuniyoshi, Y., Abe-Ouchi, A., Sherriff-Tadano, S., Chan, W.L., Saito, F., 2022. Effect of climatic precession on dansgaard-oeschger-like oscillations. Geophys. Res. Lett. 49.

Landais, A., Masson-Delmotte, V., Stenni, B., Selmo, E., Roche, D.M., Jouzel, J., Lambert, F., Guillevic, M., Bazin, L., Arzel, O., Vinther, B., Gkinis, V., Popp, T., 2015. A review of the bipolar see-saw from synchronized and high resolution ice core water stable isotope records from Greenland and East Antarctica. Quat. Sci. Rev. 114, 18–32.

Landais, A., Stenni, B., Masson-Delmotte, V., Jouzel, J., Cauquoin, A., Fourré, E., Minster, B., Selmo, E., Extier, T., Werner, M., Vimeux, F., Uemura, R., Crotti, I., Grisart, A., 2021. Interglacial Antarctic–Southern Ocean climate decoupling due to moisture source area shifts. Nat. Geosci. 14, 918–923.

Lee, S., Kim, H.-k., 2003. The dynamical relationship between subtropical and eddy-driven jets. J. Atmos. Sci. 60, 1490–1503.

Lemieux-Dudon, B., Blayo, E., Petit, J.R., Waelbroeck, C., Svensson, A., Ritz, C., Barnola, J.M., Narcisi, B.M., Parrenin, F., 2010. Consistent dating for Antarctic and Greenland ice cores. Quat. Sci. Rev. 29, 8–20.

Lin, J., Abbott, P.M., Sigl, M., Steffensen, J.P., Mulvaney, R., Severi, M., Svensson, A., 2023. Bipolar ice-core records constrain possible dates and global radiative forcing following the ~74 ka Toba eruption. Quat. Sci. Rev. 312.

Lin, J., Svensson, A., Hvidberg, C.S., Lohmann, J., Kristiansen, S., Dahl-Jensen, D., Steffensen, J.P., Rasmussen, S.O., Cook, E., Kjær, H.A., Vinther, B.M., Fischer, H., Stocker, T., Sigl, M., Bigler, M., Severi, M., Traversi, R., Mulvaney, R., 2022. Magnitude, frequency and climate forcing of global volcanism during the last glacial period as seen in Greenland and Antarctic ice cores (60–9 ka). Clim. Past 18, 485–506.

Lindzen, R.S., Hou, A.V., 1988. Hadley circulations for zonally averaged heating centered off the equator. J. Atmos. Sci. 45, 2416–2427.

Markle, B.R., Steig, E.J., Buizert, C., Schoenemann, S.W., Bitz, C.M., Fudge, T.J., Pedro, J. B., Ding, Q., Jones, T.R., White, J.W.C., Sowers, T., 2016. Global atmospheric teleconnections during Dansgaard–Oeschger events. Nat. Geosci. 10, 36–40.
Marshall, J., Speer, K., 2012. Closure of the meridional overturning circulation through Southern Ocean upwelling. Nat. Geosci. 5, 171–180.
Martin, K.C., Buizert, C., Edwards, J.S., Kalk, M.L., Riddell-Young, B., Brook, E.J., Beaudette, R., Severinghaus, J.P., Sowers, T.A., 2023. Bipolar impact and phasing of Heinrich-type climate variability. Nature 617, 100–104.
Mason, E., Edmonds, M., McConnell, J.R., 2022. Volatile trace metals deposited in ice as soluble volcanic aerosols during the 17.7.ka eruptions of Mt Takahe, West Antarctic Rift. Front. Earth Sci. 10.
McConnell, J.R., Burke, A., Dunbar, N.W., Köhler, P., Thomas, J.L., Arienzo, M.M., Chellman, N.J., Maselli, O.J., Sigl, M., Adkins, J.F., Baggenstos, D., Burkhart, J.F., Brook, E.J., Buizert, C., Cole-Dai, J., Fudge, T.J., Knorr, G., Graf, H.F., Grieman, M. M., Iverson, N., McGwire, K.C., Mulvaney, R., Paris, G., Rhodes, R.H., Saltzman, E.S., Severinghaus, J.P., Steffensen, J.P., Taylor, K.C., Winckler, G., 2017. Synchronous volcanic eruptions and abrupt climate change ~17.7 ka plausibly linked by stratospheric ozone depletion. Proc. Natl. Acad. Sci. U. S. A 114, 10035–10040.
McKay, D.I.A., Staal, A., Abrams, J.F., Winkelmann, R., Sakschewski, B., Loriani, S., Fetzer, I., Cornell, S.E., Rockström, J., Lenton, T.M., 2022. Exceeding 1.5°C global warming could trigger multiple climate tipping points. Science 377.
Muscheler, R., Beer, J., Wagner, G., Laj, C., Kissel, C., Raisbeck, G.M., Yiou, F., Kubik, P. W., 2004. Changes in the carbon cycle during the last deglaciation as indicated by the comparison of ^{10}Be and ^{14}C records. Earth Planet Sci. Lett. 219, 325–340.
Oyabu, I., Kawamura, K., Buizert, C., Parrenin, F., Orsi, A., Kitamura, K., Aoki, S., Nakazawa, T., 2022. The Dome Fuji ice core DF2021 chronology (0–207 kyr BP). Quat. Sci. Rev. 294.
Parrenin, F., Petit, J.R., Masson-Delmotte, V., Wolff, E., Basile-Doelsch, I., Jouzel, J., Lipenkov, V., Rasmussen, S.O., Schwander, J., Severi, M., Udisti, R., Veres, D., Vinther, B.M., 2012. Volcanic synchronisation between the EPICA Dome C and Vostok ice cores (Antarctica) 0-145 kyr BP. Clim. Past 8, 1031–1045.
Pedro, J.B., Jochum, M., Buizert, C., He, F., Barker, S., Rasmussen, S.O., 2018. Beyond the bipolar seesaw: toward a process understanding of interhemispheric coupling. Quat. Sci. Rev. 192, 27–46.
Peltier, W.R., Argus, D.F., Drummond, R., 2015. Space geodesy constrains ice age terminal deglaciation: the global ICE-6G-C (VM5a) model. J. Geophys. Res. Solid Earth 120, 450–487.
Peltier, W.R., Vettoretti, G., 2014. Dansgaard-Oeschger oscillations predicted in a comprehensive model of glacial climate: a "kicked" salt oscillator in the Atlantic. Geophys. Res. Lett. 41, 7306–7313.
Raisbeck, G.M., Cauquoin, A., Jouzel, J., Landais, A., Petit, J.R., Lipenkov, V.Y., Beer, J., Synal, H.A., Oerter, H., Johnsen, S.J., Steffensen, J.P., Svensson, A., Yiou, F., 2017. An improved north-south synchronization of ice core records around the 41 kyr Be-10 peak. Clim. Past 13, 217–229.
Raisbeck, G.M., Yiou, F., Jouzel, J., Stocker, T.F., 2007. Direct north-south synchronization of abrupt climate change records in ice cores using beryllium 10. Clim. Past 3, 541–547.
Ramirez, V.M., Cruz, F.W., Vuille, M., Novello, V.F., Stríkis, N.M., Cheng, H., Zhang, H. W., Bernal, J.P., Du, W.J., Ampuero, A., Deininger, M., Chiessi, C.M., Tejedor, E., Campos, J.L., Ait Brahim, Y., Edwards, R.L., 2023. Summer insolation controlled movements of Intertropical Convergence Zone during last glacial cycle in northern South America. Commun. Earth Environ. 4, 1–8.
Rasmussen, S.O., Abbott, P.M., Blunier, T., Bourne, A.J., Brook, E., Buchardt, S.L., Buizert, C., Chappellaz, J., Clausen, H.B., Cook, E., Dahl-Jensen, D., Davies, S.M., Guillevic, M., Kipfstuhl, S., Laepple, T., Seierstad, I.K., Severinghaus, J.P., Steffensen, J.P., Stowasser, C., Svensson, A., Vallelonga, P., Vinther, B.M., Wilhelms, F., Winstrup, M., 2013. A first chronology for the north Greenland eemian ice drilling (NEEM) ice core. Clim. Past. 9, 2713–2730.
Rasmussen, S.O., Bigler, M., Blockley, S.P., Blunier, T., Buchardt, S.L., Clausen, H.B., Cvijanovic, I., Dahl-Jensen, D., Johnsen, S.J., Fischer, H., Gkinis, V., Guillevic, M., Hoek, W.Z., Lowe, J.J., Pedro, J.B., Popp, T., Seierstad, I.K., Steffensen, J.P., Svensson, A.M., Vallelonga, P., Vinther, B.M., Walker, M.J.C., Wheatley, J.J., Winstrup, M., 2014. A stratigraphic framework for abrupt climatic changes during the last Glacial period based on three synchronized Greenland ice-core records: refining and extending the INTIMATE event stratigraphy. Quat. Sci. Rev. 106, 14–28.
Rhodes, R.H., Brook, E.J., Chiang, J.C.H., Blunier, T., Maselli, O.J., McConnell, J.R., Romanini, D., Severinghaus, J.P., 2015. Enhanced tropical methane production in response to iceberg discharge in the North Atlantic. Science 348, 1016–1019.
Ruth, U., Barnola, J.-M., Beer, J., Bigler, M., Blunier, T., Castellano, E., Fischer, H., Fundel, F., Huybrechts, P., Kaufmann, P., Kipfstuhl, S., Lambrecht, A., Morganti, A., Oerter, H., Parrenin, F., Rybak, O., Severi, M., Udisti, R., Wilhelms, F., Wolff, E., 2007. "EDML1": a chronology for the EPICA deep ice core from Dronning Maud Land, Antarctica, over the last 150 000 years. Clim. Past 3, 475–484.
Savarino, J., Romero, A., Cole-Dai, J., Bekki, S., Thiemens, M.H., 2003. UV induced mass-independent sulfur isotope fractionation in stratospheric volcanic sulfate. Geophys. Res. Lett. 30, ASC11–ASC12.
Schindlbeck-Belo, J.C., Toohey, M., Jegen, M., Kutterolf, S., Rehfeld, K., 2024. PalVol v1: a proxy-based semi-stochastic ensemble reconstruction of volcanic stratospheric sulfur injection for the last glacial cycle (140000-50BP). Earth Syst. Sci. Data 16, 1063–1081.
Schmidt, G.A., LeGrande, A.N., Hoffmann, G., 2007. Water isotope expressions of intrinsic and forced variability in a coupled ocean-atmosphere model. J. Geophys. Res. Atmos. 112.
Schneider, T., Bischoff, T., Haug, G.H., 2014. Migrations and dynamics of the intertropical convergence zone. Nature 513, 45–53.
Schwander, J., Stauffer, B., 1984. Age difference between polar ice and the air trapped in its bubbles. Nature 311, 45–47.
Seierstad, I.K., Abbott, P.M., Bigler, M., Blunier, T., Bourne, A.J., Brook, E., Buchardt, S. L., Buizert, C., Clausen, H.B., Cook, E., Dahl-Jensen, D., Davies, S.M., Guillevic, M., Johnsen, S.J., Pedersen, D.S., Popp, T.J., Rasmussen, S.O., Severinghaus, J.P., Svensson, A., Vinther, B.M., 2014. Consistently dated records from the Greenland GRIP, GISP2 and NGRIP ice cores for the past 104 ka reveal regional millennial-scale delta O-18 gradients with possible Heinrich event imprint. Quat. Sci. Rev. 106, 29–46.
Severi, M., Becagli, S., Castellano, E., Morganti, A., Traversi, R., Udisti, R., Ruth, U., Fischer, H., Huybrechts, P., Wolff, E., Parrenin, F., Kaufmann, P., Lambert, F., Steffensen, J.P., 2007. Synchronisation of the EDML and EDC ice cores for the last 52 kyr by volcanic signature matching. Clim. Past 3, 367–374.
Severi, M., Udisti, R., Becagli, S., Stenni, B., Traversi, R., 2012. Volcanic synchronisation of the EPICA-DC and TALDICE ice cores for the last 42 kyr BP. Clim. Past. 8, 509–517.
Shields, C.A., Bailey, D.A., Danabasoglu, G., Jochum, M., Kiehl, J.T., Levis, S., Park, S., 2012. The low-resolution CCSM4. J. Clim. 25, 3993–4014.
Shin, Y., Kang, S.M., 2021. How does the high-latitude thermal forcing in one hemisphere affect the other hemisphere? Geophys. Res. Lett. 48 e2021GL095870.
Shin, Y., Kang, S.M., Takahashi, K., Stuecker, M.F., Hwang, Y.-T., Kim, D., 2021. Evolution of the tropical response to periodic extratropical thermal forcing. J. Clim. 34, 6335–6353.
Sigl, M., Winstrup, M., McConnell, J.R., Welten, K.C., Plunkett, G., Ludlow, F., Büntgen, U., Caffee, M., Chellman, N., Dahl-Jensen, D., Fischer, H., Kipfstuhl, S., Kostick, C., Maselli, O.J., Mekhaldi, F., Mulvaney, R., Muscheler, R., Pasteris, D.R., Pilcher, J.R., Salzer, M., Schüpbach, S., Steffensen, J.P., Vinther, B.M., Woodruff, T. E., 2015. Timing and climate forcing of volcanic eruptions for the past 2,500 years. Nature 523, 543–549.
Sinnl, G., Adolphi, F., Christl, M., Welten, K.C., Woodruff, T., Caffee, M., Svensson, A., Muscheler, R., Rasmussen, S.O., 2023. Synchronizing ice-core and U / Th timescales in the Last Glacial Maximum uslng Hulu Cave 14C and new 10Be measurements from Greenland and Antarctica. Clim. Past 19, 1153–1175.
Stocker, T.F., Johnsen, S.J., 2003. A minimum thermodynamic model for the bipolar seesaw. Paleoceanography 18.
Svensson, A., Andersen, K.K., Bigler, M., Clausen, H.B., Dahl-Jensen, D., Davies, S.M., Johnsen, S.J., Muscheler, R., Parrenin, F., Rasmussen, S.O., Röthlisberger, R., Seierstad, I., Steffensen, J.P., Vinther, B.M., 2008. A 60 000 year Greenland stratigraphic ice core chronology. Clim. Past 4, 47–57.
Svensson, A., Bigler, M., Blunier, T., Clausen, H.B., Dahl-Jensen, D., Fischer, H., Fujita, S., Goto-Azuma, K., Johnsen, S.J., Kawamura, K., Kipfstuhl, S., Kohno, M., Parrenin, F., Popp, T., Rasmussen, S.O., Schwander, J., Seierstad, I., Severi, M., Steffensen, J.P., Udisti, R., Uemura, R., Vallelonga, P., Vinther, B.M., Wegner, A., Wilhelms, F., Winstrup, M., 2013. Direct linking of Greenland and Antarctic ice cores at the Toba eruption (74 ka BP). Clim. Past 9, 749–766.
Svensson, A., Bigler, M., Kettner, E., Dahl-Jensen, D., Johnsen, S., Kipfstuhl, S., Nielsen, M., Steffensen, J.P., 2011. Annual layering in the NGRIP ice core during the Eemian. Clim. Past 7, 1427–1437.
Svensson, A., Dahl-Jensen, D., Steffensen, J.P., Blunier, T., Rasmussen, S.O., Vinther, B. M., Vallelonga, P., Capron, E., Gkinis, V., Cook, E., Kjær, H.A., Muscheler, R., Kipfstuhl, S., Wilhelms, F., Stocker, T.F., Fischer, H., Adolphi, F., Erhardt, T., Sigl, M., Landais, A., Parrenin, F., Buizert, C., McConnell, J.R., Severi, M., Mulvaney, R., Bigler, M., 2020. Bipolar volcanic synchronization of abrupt climate change in Greenland and Antarctic ice cores during the last glacial period. Clim. Past 16, 1565–1580.
Trenberth, K.E., Fasullo, J.T., 2017. Atlantic meridional heat transports computed from balancing Earth's energy locally. Geophys. Res. Lett. 44, 1919–1927.
Uemura, R., Masson-Delmotte, V., Jouzel, J., Landais, A., Motoyama, H., Stenni, B., 2012. Ranges of moisture-source temperature estimated from Antarctic ice cores stable isotope records over glacial-interglacial cycles. Clim. Past 8, 1109–1125.
Vallelonga, P., Bertagna, G., Blunier, T., Kjaer, H.A., Popp, T.J., Rasmussen, S.O., Steffensen, J.P., Stowasser, C., Svensson, A.S., Warming, E., Winstrup, M., Bigler, M., Kipfstuhl, S., 2012. Duration of Greenland Stadial 22 and ice-gas Delta age from counting of annual layers in Greenland NGRIP ice core. Clim. Past 8, 1839–1847.
Vallis, G.K., 2017. Atmospheric and Oceanic Fluid Dynamics: Fundamentals and Large-Scale Circulation, 2 ed. Cambridge University Press, Cambridge.
Veres, D., Bazin, L., Landais, A., Toyé Mahamadou Kele, H., Lemieux-Dudon, B., Parrenin, F., Martinerie, P., Blayo, E., Blunier, T., Capron, E., Chappellaz, J., Rasmussen, S.O., Severi, M., Svensson, A., Vinther, B., Wolff, E.W., 2013. The Antarctic ice core chronology (AICC2012): an optimized multi-parameter and multi-site dating approach for the last 120 thousand years. Clim. Past 9, 1733–1748.
Vettoretti, G., Ditlevsen, P., Jochum, M., Rasmussen, S.O., 2022. Atmospheric CO2 control of spontaneous millennial-scale ice age climate oscillations. Nat. Geosci. 15, 300–306.
Vettoretti, G., Peltier, W.R., 2016. Thermohaline instability and the formation of glacial North Atlantic super polynyas at the onset of Dansgaard-Oeschger warming events. Geophys. Res. Lett. 43, 5336–5344.
Vettoretti, G., Peltier, W.R., 2018. Fast physics and slow physics in the nonlinear dansgaard–oeschger relaxation oscillation. J. Clim. 31, 3423–3449.
Wagner, G., Beer, J., Masarik, J., Muscheler, R., Kubik, P.W., Mende, W., Laj, C., Raisbeck, G.M., Yiou, F., 2001. Presence of the solar de Vries cycle (~205 years) during the last ice age. Geophys. Res. Lett. 28, 303–306.
WAIS Divide Project Members, 2013. Onset of deglacial warming in West Antarctica driven by local orbital forcing. Nature 500, 440–444.
WAIS Divide Project Members, 2015. Precise interpolar phasing of abrupt climate change during the last ice age. Nature 520, 661-U169.

Wang, S., Foster, A., Lenz, E.A., Kessler, J.D., Stroeve, J.C., Anderson, L.O., Turetsky, M., Betts, R., Zou, S., Liu, W., Boos, W.R., Hausfather, Z., 2023. Mechanisms and impacts of Earth System tipping elements. Rev. Geophys. 61.
Wolff, E.W., Burke, A., Crick, L., Doyle, E.A., Innes, H.M., Mahony, S.H., Rae, J.W.B., Severi, M., Sparks, R.S.J., 2023. Frequency of large volcanic eruptions over the past 200 000 years. Clim. Past 19, 23–33.
Wolff, E.W., Chappellaz, J., Blunier, T., Rasmussen, S.O., Svensson, A., 2010. Millennial-scale variability during the last glacial: the ice core record. Quat. Sci. Rev. 29, 2828–2838.
Yiou, F., Raisbeck, G.M., Baumgartner, S., Beer, J., Hammer, C., Johnsen, S., Jouzel, J., Kubik, P.W., Lestringuez, J., Stiévenard, M., Suter, M., Yiou, P., 1997. Beryllium 10 in Greenland Ice Core Project ice core at Summit, Greenland. J. Geophys. Res. 102, 26783–26794.
Zreda-Gostynska, G., Kyle, P.R., Finnegan, D., Prestbo, K.M., 1997. Volcanic gas emissions from Mount Erebus and their impact on the Antarctic environment. J. Geophys. Res. Solid Earth 102, 15039–15055.

Further Reading

Alley, et al., 1993. Abrupt increase in Greenland snow accumulation at the end of the younger Dryas event. Nature 362, 527–529.
Beer, J., McCracken, K.G., Adolphi, F., Christl, M., Fischer, H., Miller, H., Muscheler, R., Synal, H.A., Wilhelms, F., 2025. Heliomagnetic and geomagnetic activity cycles on millennial timescales. Quat. Sci. Rev. 361.
Bigler, M., 2004. Hochauflösende Spurenstoffmessungen an Polaren Eisbohrkernen: Glazio-Chemische Und Klimatische Prozessstudien, Physics Institute. University of Bern, Switzerland.
Dahl-Jensen, D., Gundestrup, N., Miller, H., Watanabe, O., Johnsen, S.J., Steffensen, J.P., Clausen, H.B., Svensson, A., Larsen, L.B., 2002. The NorthGRIP deep drilling program. Ann. Glaciol. 35, 1–4.
Dansgaard, W., Johnsen, S.J., Clausen, H.B., Dahl-Jensen, D., Gundestrup, N.S., Hammer, C.U., Hvidberg, C.S., Steffensen, J.P., Sveinbjörnsdottir, A.E., Jouzel, J., Bond, G., 1993. Evidence for general instability of past climate from a 250-kyr ice-core record. Nature 364, 218–220.
EPICA community members, 2004. Eight glacial cycles from an Antarctic ice core. Nature 429, 623–628.
EPICA community members, 2006. One-to-one coupling of glacial climate variability in Greeland and Antartctica. Nature 444, 195–198.
Erhardt, T., Bigler, M., Federer, U., Gfeller, G., Leuenberger, D., Stowasser, O., Röthlisberger, R., Schüpbach, S., Ruth, U., Twarloh, B., Wegner, A., Goto-Azuma, K., Kuramoto, T., Kjær, H.A., Vallelonga, P.T., Siggaard-Andersen, M.L., Hansson, M.E., Benton, A.K., Fleet, L.G., Mulvaney, R., Thomas, E.R., Abram, N., Stocker, T.F., Fischer, H., 2022. High-resolution aerosol concentration data from the Greenland NorthGRIP and NEEM deep ice cores. Earth Syst. Sci. Data 14, 1215–1231.
Faria, S.H., Kipfstuhl, S., Lambrecht, A., Faria, S.H., Kipfstuhl, S., Lambrecht, A., 2018. EPICA-DML Deep Ice Core: a Visual Record, Epica-Dml Deep Ice Core: a Visual Record.
Fudge, T.J., Taylor, K.C., Waddington, E.D., Fitzpatrick, J.J., Conway, H., 2016. Electrical stratigraphy of the WAIS divide ice core: identification of centimeter-scale irregular layering. J. Geophys. Res.: Earth Surf. 121, 1218–1229.
Fujita, S., Azuma, N., Motoyama, H., Kameda, T., Narita, H., Fujii, Y., Watanabe, O., 2002. Electrical measurements on the 2503 m Dome F Antarctic ice core. Ann. Glaciol. 35, 313–320.
Gkinis, V., Simonsen, S.B., Buchardt, S.L., White, J.W.C., Vinther, B.M., 2014. Water isotope diffusion rates from the NorthGRIP ice core for the last 16,000 years – glaciological and paleoclimatic implications. Earth Planet Sci. Lett. 405, 132–141.
Gkinis, V., Vinther, B.M., Popp, T.J., Quistgaard, T., Faber, A.-K., Holme, C.T., Jensen, C.-M., Lanzky, M., Lütt, A.-M., Mandrakis, V., Ørum, N.-O., Pedersen, A.-S., Vaxevani, N., Weng, Y., Capron, E., Dahl-Jensen, D., Hörhold, M., Jones, T.R., Jouzel, J., Landais, A., Masson-Delmotte, V., Oerter, H., Rasmussen, S.O., Steen-Larsen, H.C., Steffensen, J.-P., Sveinbjörnsdóttir, Á.-E., Svensson, A., Vaughn, B., White, J.W.C., 2021. A 120,000-year long climate record from a NW-Greenland deep ice core at ultra-high resolution. Sci. Data 8, 141.
Greenland Ice-Core Project (GRIP) Members, 1993. Climate instability during the last interglacial period recorded in the GRIP ice core. Nature 364, 203–207.
Grootes, P.M., Stuiver, M., White, J.W.C., Johnsen, S.J., Jouzel, J., 1993. Comparison of oxygen isotope records from the GISP2 and GRIP Greenland ice cores. Nature 366, 552–554.
Johnsen, S.J., DahlJensen, D., Gundestrup, N., Steffensen, J.P., Clausen, H.B., Miller, H., Masson-Delmotte, V., Sveinbjornsdottir, A.E., White, J., 2001. Oxygen isotope and palaeotemperature records from six Greenland ice-core stations: camp century, Dye-3, GRIP, GISP2, Renland and NorthGRIP. J. Quat. Sci. 16, 299–307.
Kawamura, K., Parrenin, F., Lisiecki, L., Uemura, R., Vimeux, F., Severinghaus, J.P., Hutterli, M.A., Nakazawa, T., Aoki, S., Jouzel, J., Raymo, M.E., Matsumoto, K., Nakata, H., Motoyama, H., Fujita, S., Goto-Azuma, K., Fujii, Y., Watanabe, O., 2007. Northern Hemisphere forcing of climatic cycles in Antarctica over the past 360,000 years. Nature 448, 912–U914.
Landais, A., Masson-Delmotte, V., Stenni, B., Selmo, E., Roche, D.M., Jouzel, J., Lambert, F., Guillevic, M., Bazin, L., Arzel, O., Vinther, B., Gkinis, V., Popp, T., 2015. A review of the bipolar see-saw from synchronized and high resolution ice core water stable isotope records from Greenland and East Antarctica. Quat. Sci. Rev. 114, 18–32.
Landais, A., Stenni, B., Masson-Delmotte, V., Jouzel, J., Cauquoin, A., Fourré, E., Minster, B., Selmo, E., Extier, T., Werner, M., Vimeux, F., Uemura, R., Crotti, I., Grisart, A., 2021. Interglacial Antarctic–Southern Ocean climate decoupling due to moisture source area shifts. Nat. Geosci. 14, 918–923.
Lin, J., Svensson, A., Hvidberg, C.S., Lohmann, J., Kristiansen, S., Dahl-Jensen, D., Steffensen, J.P., Rasmussen, S.O., Cook, E., Kjær, H.A., Vinther, B.M., Fischer, H., Stocker, T., Sigl, M., Bigler, M., Severi, M., Traversi, R., Mulvaney, R., 2022. Magnitude, frequency and climate forcing of global volcanism during the last glacial period as seen in Greenland and Antarctic ice cores (60–9 ka). Clim. Past 18, 485–506.
Markle, B.R., Steig, E.J., Buizert, C., Schoenemann, S.W., Bitz, C.M., Fudge, T.J., Pedro, J. B., Ding, Q., Jones, T.R., White, J.W.C., Sowers, T., 2016. Global atmospheric teleconnections during Dansgaard–Oeschger events. Nat. Geosci. 10, 36–40.
Mayewski, P.A., Meeker, L.D., Twickler, M.S., Whitlow, S., Yang, Q.Z., Lyons, W.B., Prentice, M., 1997. Major features and forcing of high-latitude northern hemisphere atmospheric circulation using a 110,000-year-long glaciochemical series. Journal of Geophysical Research-Oceans 102, 26345–26366.
Muscheler, R., Beer, J., Wagner, G., Laj, C., Kissel, C., Raisbeck, G.M., Yiou, F., Kubik, P. W., 2004. Changes in the carbon cycle during the last deglaciation as indicated by the comparison of 10Be and 14C records. Earth Planet Sci. Lett. 219, 325–340.
NEEM community members, 2013. Eemian interglacial reconstructed from a Greenland folded ice core. Nature 493, 489–494.
North Greenland Ice Core Project members, 2004. High-resolution record of Northern Hemisphere climate extending into the last interglacial period. Nature 431, 147–151.
Parrenin, F., Petit, J.R., Masson-Delmotte, V., Wolff, E., Basile-Doelsch, I., Jouzel, J., Lipenkov, V., Rasmussen, S.O., Schwander, J., Severi, M., Udisti, R., Veres, D., Vinther, B.M., 2012. Volcanic synchronisation between the EPICA Dome C and Vostok ice cores (Antarctica) 0-145 kyr BP. Clim. Past 8, 1031–1045.
Rasmussen, S.O., Abbott, P.M., Blunier, T., Bourne, A.J., Brook, E., Buchardt, S.L., Buizert, C., Chappellaz, J., Clausen, H.B., Cook, E., Dahl-Jensen, D., Davies, S.M., Guillevic, M., Kipfstuhl, S., Laepple, T., Seierstad, I.K., Severinghaus, J.P., Steffensen, J.P., Stowasser, C., Svensson, A., Vallelonga, P., Vinther, B.M., Wilhelms, F., Winstrup, M., 2013. A first chronology for the north Greenland eemian ice drilling (NEEM) ice core. Clim. Past. 9, 2713–2730.
Rasmussen, S.O., Dahl-Jensen, D., Fischer, H., Fuhrer, K., Hansen, S.B., Hansson, M., Hvidberg, C.S., Jonsell, U., Kipfstuhl, S., Ruth, U., Schwander, J., Siggaard-Andersen, M.L., Sinnl, G., Steffensen, J.P., Svensson, A.M., Vinther, B.M., 2023. Ice-core data used for the construction of the Greenland Ice-Core Chronology 2005 and 2021 (GICC05 and GICC21). Earth Syst. Sci. Data 15, 3351–3364.
Ruth, U., Barnola, J.-M., Beer, J., Bigler, M., Blunier, T., Castellano, E., Fischer, H., Fundel, F., Huybrechts, P., Kaufmann, P., Kipfstuhl, S., Lambrecht, A., Morganti, A., Oerter, H., Parrenin, F., Rybak, O., Severi, M., Udisti, R., Wilhelms, F., Wolff, E., 2007. "EDML1": a chronology for the EPICA deep ice core from Dronning Maud Land, Antarctica, over the last 150 000 years. Clim. Past 3, 475–484.
Ruth, U., Wagenbach, D., Steffensen, J.P., Bigler, M., 2003. Continuous record of microparticle concentration and size distribution in the central Greenland NGRIP ice core during the last glacial period. J. Geophys. Res. 108.
Schüpbach, S., Fischer, H., Bigler, M., Erhardt, T., Gfeller, G., Leuenberger, D., Mini, O., Mulvaney, R., Abram, N.J., Fleet, L., Frey, M.M., Thomas, E., Svensson, A., Dahl-Jensen, D., Kettner, E., Kjaer, H., Seierstad, I., Steffensen, J.P., Rasmussen, S.O., Vallelonga, P., Winstrup, M., Wegner, A., Twarloh, B., Wolff, K., Schmidt, K., Goto-Azuma, K., Kuramoto, T., Hirabayashi, M., Uetake, J., Zheng, J., Bourgeois, J., Fisher, D., Zhiheng, D., Xiao, C., Legrand, M., Spolaor, A., Gabrieli, J., Barbante, C., Kang, J.H., Hur, S.D., Hong, S.B., Hwang, H.J., Hong, S., Hansson, M., Iizuka, Y., Oyabu, I., Muscheler, R., Adolphi, F., Maselli, O., McConnell, J., Wolff, E.W., 2018. Greenland records of aerosol source and atmospheric lifetime changes from the Eemian to the Holocene. Nat. Commun. 9.
Severi, M., Becagli, S., Castellano, E., Morganti, A., Traversi, R., Udisti, R., Ruth, U., Fischer, H., Huybrechts, P., Wolff, E., Parrenin, F., Kaufmann, P., Lambert, F., Steffensen, J.P., 2007. Synchronisation of the EDML and EDC ice cores for the last 52 kyr by volcanic signature matching. Clim. Past 3, 367–374.
Sigl, M., Fudge, T.J., Winstrup, M., Cole-Dai, J., Ferris, D., McConnell, J.R., Taylor, K.C., Welten, K.C., Woodruff, T.E., Adolphi, F., Bisiaux, M., Brook, E.J., Buizert, C., Caffee, M.W., Dunbar, N.W., Edwards, R., Geng, L., Iverson, N., Koffman, B., Layman, L., Maselli, O.J., McGwire, K., Muscheler, R., Nishiizumi, K., Pasteris, D.R., Rhodes, R.H., Sowers, T.A., 2016. The WAIS Divide deep ice core WD2014 chronology - part 2: Annual-layer counting (0-31 ka BP). Clim. Past. 12, 769–786.
Stenni, B., Buiron, D., Frezzotti, M., Albani, S., Barbante, C., Bard, E., Barnola, J.M., Baroni, M., Baumgartner, M., Bonazza, M., Capron, E., Castellano, E., Chappellaz, J., Delmonte, B., Falourd, S., Genoni, L., Iacumin, P., Jouzel, J., Kipfstuhl, S., Landais, A., Lemieux-Dudon, B., Maggi, V., Masson-Delmotte, V., Mazzola, C., Minster, B., Montagnat, M., Mulvaney, R., Narcisi, B., Oerter, H., Parrenin, F., Petit, J.R., Ritz, C., Scarchilli, C., Schilt, A., Schupbach, S., Schwander, J., Selmo, E., Severi, M., Stocker, T.F., Udisti, R., 2010a. Expression of the bipolar see-saw in Antarctic climate records during the last deglaciation. Nat. Geosci. 4, 46–49.
Stenni, B., Masson-Delmotte, V., Selmo, E., Oerter, H., Meyer, H., Röthlisberger, R., Jouzel, J., Cattani, O., Falourd, S., Fischer, H., Hoffmann, G., Iacumin, P., Johnsen, S. J., Minster, B., Udisti, R., 2010b. The deuterium excess records of EPICA Dome C and Dronning Maud Land ice cores (East Antarctica). Quat. Sci. Rev. 29, 146–159.
Stuiver, M., Grootes, P.M., 2000. GISP2 oxygen isotope ratios. Quaternary Research 53, 277–284.
Svensson, A., Nielsen, S.W., Kipfstuhl, S., Johnsen, S.J., Steffensen, J.P., Bigler, M., Ruth, U., Röthlisberger, R., 2005. Visual stratigraphy of the North Greenland Ice Core Project (NorthGRIP) ice core during the last glacial period. J. Geophys. Res. Atmos. 110, 1–11.
Taylor, K.C., Alley, R.B., Lamorey, G.W., Mayewski, P., 1997. Electrical measurements on the Greenland Ice Sheet Project 2 Core. J. Geophys. Res. 102, 26511–26517.

Uemura, R., Motoyama, H., Masson-Delmotte, V., Jouzel, J., Kawamura, K., Goto-Azuma, K., Fujita, S., Kuramoto, T., Hirabayashi, M., Miyake, T., Ohno, H., Fujita, K., Abe-Ouchi, A., Iizuka, Y., Horikawa, S., Igarashi, M., Suzuki, K., Suzuki, T., Fujii, Y., 2018. Asynchrony between Antarctic temperature and CO2 associated with obliquity over the past 720,000 years. Nat. Commun. 9, 961.

Wagner, G., Beer, J., Masarik, J., Muscheler, R., Kubik, P.W., Mende, W., Laj, C., Raisbeck, G.M., Yiou, F., 2001. Presence of the solar de Vries cycle (~205 years) during the last ice age. Geophys. Res. Lett. 28, 303–306.

WAIS Divide Project Members, 2013. Onset of deglacial warming in West Antarctica driven by local orbital forcing. Nature 500, 440–444.

WAIS Divide Project Members, 2015. Precise interpolar phasing of abrupt climate change during the last ice age. Nature 520, 661. U169.

Wolff, E.W., Moore, J.C., Clausen, H.B., Hammer, C.U., 1997. Climatic implications of background acidity and other chemistry derived from electrical studies of the Greenland ice core Project ice core. J. Geophys. Res. 102, 26325–26332.

Yiou, F., Raisbeck, G.M., Baumgartner, S., Beer, J., Hammer, C., Johnsen, S., Jouzel, J., Kubik, P.W., Lestringuez, J., Stiévenard, M., Suter, M., Yiou, P., 1997. Beryllium 10 in Greenland Ice core Project ice core at Summit, Greenland. J. Geophys. Res. 102, 26783–26794.